Spring 5-2015

Marine Snow Settling Velocities at an Oil Spill Site and a Control Site in the Northern Gulf of Mexico

Clayton Hugh Dike
University of Southern Mississippi

The University of Southern Mississippi

MARINE SNOW SETTLING VELOCITIES AT AN OIL SPILL SITE AND A CONTROL SITE IN THE NORTHERN GULF OF MEXICO

by

Clayton Hugh Dike

A Thesis
Submitted to the Graduate School
of The University of Southern Mississippi
in Partial Fulfillment of the Requirements
for the Degree of Master of Science

Approved:

Dr. Vernon Asper
Committee Chair

Dr. Arne Diercks

Dr. William "Monty" Graham

Dr. Karen Coats
Dean of the Graduate School

May 2015

ABSTRACT

MARINE SNOW SETTLING VELOCITIES AT AN OIL SPILL SITE AND A CONTROL SITE IN THE NORTHERN GULF OF MEXICO

by Clayton Hugh Dike

May 2015

After budgeting for response efforts and natural processes, over one million barrels of oil from the BP oil spill were unaccounted for. A hypothesis coined "The Dirty Blizzard" formed subsequent to observations of large and numerous oiled marine snow aggregates amidst the surface slick proposed that a large quantity of oil sank to depth via the aggregates. Having reached the seafloor, aggregates were subject to microbial degradation and to redistribution due to bottom currents. To assist in characterizing redistribution of particles near the seafloor, sediment traps, marine snow cameras, and acoustic Doppler current profilers (ADCPs) were deployed at two sites below the continental shelf break. One site was underneath the oiling footprint near the location of the Deepwater Horizon wellhead and another site was away from the oiling footprint in an area of observed natural seepage. Since oiled particles presumably contained constituents dense enough to sink buoyant oil, which continued to degrade leaving behind relatively heavy components, it was hypothesized that particles at the oiled site would have faster settling velocities than particles at the unoiled site. Using data from the ADCPs, the sediment traps, and the marine snow profiling cameras, an examination of particle sources is undertaken. Marine snow was not found to be denser underneath the oiling footprint, and marine snow flux periodicities did not match current periodicities.

DEDICATION

This thesis is dedicated to Jennifer Paddock, whom I will always remember.

ACKNOWLEDGMENTS

Special thanks goes to my committee chair, Dr. Vernon Asper, and my other committee members, Dr. Arne Diercks, and Dr. William “Monty” Graham, for their advice and support throughout the duration of this research.

I would also like to thank Jeanne Stewart for the help in creating this document.

TABLE OF CONTENTS

LIST OF TABLES

Table

LIST OF ILLUSTRATIONS

Figure

CHAPTER I

BACKGROUND

BP Oil Spill

Accounting of the Spill Oil

Missing oil. The BP oil spill is considered the largest oil spill in U.S. history (Gulf Oil Spill). It was the largest and deepest accidental release of oil and gas into the ocean and was accompanied with the largest application of dispersant, which was applied both at the surface and at depth (Hastings et al., 2014). BP's *Deepwater Horizon* drilling platform located at MC252 exploded, releasing almost 5 million barrels of oil into the Gulf of Mexico before the well could be capped (Demes et al., 2013) after 87 days (Fisher et al., 2014). The *Deepwater Horizon* wellhead was in about 1,540 m of water. In the water column, oil can be transported, dispersed, weathered, emulsified, and transformed biochemically (Tansel, 2014). A surface slick formed that on one day covered 141,581 km^2, for ten days covered 42,023 km^2, and for thirty days covered 14,357 km^2 (Crowsey, 2013). Of the oil released into the Gulf, 41% was removed by the response effort via dispersion, burning, and skimming and 37% was estimated to have disappeared naturally by dispersion, evaporation, and dissolution (Table 1). As 22% of the spilled oil was unaccounted for, remnants of the surface oil may continue to affect the complex network of interacting factors comprising the ecosystem (Demes et al., 2013). Much of the oil ended up in the deep sea (Fisher et al., 2014).

Table 1

Accounting of Spill Oil (Ramseur, 2010)

Removal Method	Millions of Barrels
1. Chemically dispersed	0.770
2. Burned	0.260
3. Skimmed	0.160
4. Direct recovery from the wellhead	0.820
5. Natural dispersion	0.630
6. Evaporated or dissolved	1.2
7. Total accounted oil (remainder)	3.84 (1.1)

Oil Spill Recovery

Toxins. The impacts of oil spills vary depending on oil type, incident location, oil quantity, spill rate, weather conditions, and response effort (Demes et al., 2013). As no two types of crude oil are the same, accurate impact predictions are impossible as oil toxicity depends on many factors including physical and chemical oil characteristics, bioavailability and weathering of the oil, and routes and regimes of exposure (Demes et al., 2013). Crude oil contains naphthenic acid, a mixture of carboxylic acids, which affects biota based on individual characteristics such as food consumption, life history stage, physiological demands, and exposure levels (Demes et al., 2013). Studies of the oil spill have found spatial and temporal distributions of dissolved and dispersed aromatic hydrocarbons, toxic constituents that affect marine organisms, in the water column (Demes et al., 2013). Polycyclic aromatic hydrocarbons (PAHs) are persistent aromatic hydrocarbons with two or more benzene rings that accumulate in marine sediment (Dong

et al., 2014). Although fish are able to process and eliminate oil, shrimp and crabs are affected by PAHs, and oysters and clams are even more so (NOAA FISHERIES, 2012). Hydrocarbons have been suspected to negatively impact foraminifers (Cruz, 2014).

Research findings. What part of the deep sea is impacted by toxic oil constituents is one question, but another is what toxic constituents are left when oil enters a community? After the "dirty blizzard," down core changes in the metals Mn, Re and Cd were found indicating more reducing conditions (Hastings et al., 2014). Double peaks of Mn were observed, indicative of a shoaling redox cline and a relic Mn peak, due to organic carbon input which was possibly more labile than pre spill carbon (Hastings et al., 2014). Toxic oil residual such as PAHs may remain in the water column for years. Although a study in the Arctic found bio attenuation of PAHs as bacteria were living in cold, dark, deep, and oligotrophic sediment (Dong et al., 2014), PAHs may continue to affect communities. The moderately contaminating level of PAHs begins at 1,000 $ng \cdot g^{-1}$ and becomes highly contaminating at >4,000 $ng \cdot g^{-1}$ (Cruz, 2014). A sediment study of the continental shelf in the northern Gulf of Mexico found PAH levels to be relatively low, with lower concentrations found near the spill site than concentrations found in the eastern and western Gulf (Martinec et al., 2014). However, it was found that deep sea meiofauna populations became less diverse, although total numbers did not change much, as a result of the spill (Deep Sea Ecosystem May Take Decades to Recover from Deepwater Horizon Spill, 2013). Decreased depth of habitation of foraminifers was found at a polluted site (Cruz, 2014). Opportunistic species may increase in density, as CRUZ, 2014 found evidence of foraminifera hypertrophy in 2010 at an oiled site about 15 km west of the spill site, with signs of recovery the following year. Benthic foraminifers' density was found to decrease with more reducing sediment (Hastings et al.,

2014). Oil from the spill suffocated tube worms (Borenstein, 2011). Adverse oil spill effects were discovered amongst coral below 1,000 m to include *Paramuricea biscaya* found at 2 sites, MC297 and MC294 (Fisher et al., 2014).

Recovery. Although complete recovery is expected (Demes et al., 2013), time scales and damage extents are indeterminate due to the incomplete accounting of spill oil. Ecological community recovery is dependent on the level of disturbance, characteristics of habitat, and assortment of species (Demes et al., 2013). The residence time of oil in the marine environment is dependent on hydrodynamics and degradation as removal processes; yet microbial remediation will ultimately get rid of remaining oil (Demes et al., 2013). Bacteria can assimilate hydrocarbons and some aromatic hydrocarbon isomers, but not all high molecular weight fractions. Depending on natural processes of local ecosystems, recovery rates can vary from a year to twenty years and are likely related to generation times as short lived species may recover in a matter of years, likely becoming dominant community constituents (Demes et al., 2013). Plankton, having a generation time of hours to days, is expected to quickly recover and bivalves will recover in five to ten years after oiling (Demes et al., 2013). However, ecological interactions may shift, complicating recovery time, and the impact of oil on complex ecological interactions is not understood at the community level (Demes et al., 2013). In 2012, a Mn double peak disappeared from a site from which a time series of core samples were taken indicating possible surface sediment recovery, and Re was shown to have decreased at two sites in 2013, indicating possible recovery (Hastings et al., 2014).

Valdez and IXTOC I. The environment has not recovered from the Exxon Valdez spill (Armstrong & Wilson, 2013) or the IXTOC-I oil spill. Several species have not recovered due to lingering effects of Exxon's oil spill including herring, pigeon

guillemots (NOAA, 2015), and a group of killer whales likely to go extinct (Shigenaka, 2014). The herring provide food for otters, seals, whales, and birds (Elliot & Penaloza, 2014). Their demise is not well understood, but perhaps is a result of the ecosystem having recovered in a different mode (Elliot & Penaloza, 2014). Twenty years after the spill, sea otters, sea ducks, and sea birds were producing an enzyme as a result of oil exposure (Pemberton, 2010). Subsurface oil that is highly odiferous, lightly weathered, and very fluid may remain for many years in a toxic form that can become bioavailable if disturbed (Exxon Valdez oil spill, 2010). Many studies concluded that in the case of the IXTOC-I oil spill, environmental effects were dampened by evaporation, dispersion, photo-oxidation and biodegradation of the oil, yet oil remained in the water and in the sediment (Soto et al., 2014). The IXTOC-I spill showed that the pelagic realm recovered more quickly than the benthic, but a lack of baseline data has hindered environmental assessment of that oil spill, the effects of which have been obfuscated by continuing inputs of hydrocarbons into the southwest region of the Gulf of Mexico by PEMEX oil operations (Soto et al., 2014).

Redistribution

Marine Snow and Surface Oil

Overview. Marine snow is found throughout the world's oceans and transports material out of the upper ocean at a rate of 100s meters per day (Passow, Ziervogel, Asper, & Diercks, 2012). Aggregations of mucilaginous plant and bacterial product develop in the surface ocean. Nutrients and carbon that become constituents of these aggregates may provide the foundation of small ecosystems as aggregate bound bacteria metabolize the constituents, and aggregated nutrients may become more available to surface consumers. Subject to mixing forces, these sticky aggregates can agglutinate

with other aggregates and suspended material, possibly becoming dense enough to sink. Sinking aggregates can contain phytoplankton debris and particle-associated bacteria (Joye, Teske, & Kostka, 2014). Particles that settle fast enough are able to sink below the mixed layer before they are biologically degraded. Sedimentation of biological particles is an important mechanism for transporting atmospheric CO_2, carbon, and nutrients to depth (Jouandet et al., 2014), and sinking organic particles are partly responsible for atmospheric CO_2 reduction as they transport ~10 gigatonnes of carbon yearly (Mayor, Sanders, Giering, & Anderson, 2014). The transported carbon may be confined to deep-water circulation for 500–1000 years as a function of, in part, particulate carbon transformation by microbes and zooplankton (Jouandet et al., 2014).

Dirty blizzard. Of the 1.078 million barrels of oil that were not accounted for, a significant portion may have been transported from the surface to depth via aggregation. Large, cm sized, marine snow aggregates were observed to have formed on the surface in the oil slick (Passow, Ziervogel, Asper, & Diercks, 2012), conceivably transporting a significant amount of oil to depth upon sinking (Figure 1). Tarry aggregates may have formed with sediment material at the surface causing the oil to sink days after the spill (Demes et al., 2013). Passow et al., 2012 hypothesized spill oil may have increased surface aggregate production by three mechanisms: 1) oil-degraders produced webs of mucous at the surface (Figure 1), 2) oil components interacted with suspended matter producing oily matter and coagulations (Figure 1), and 3) oil coagulated with phytoplankton. Oil-derived aggregates showed increased carbohydrate-degrading enzyme activity as they entrapped and emulsified oil within a mesh of extracellular polysaccharides, becoming a locus for microbial hydrocarbon degradation, allowing biodegradation throughout the journey from the surface to the seafloor (Joye et al., 2014).

These aggregates were precursors to oil-derived material that fell to the seafloor during the summer and fall of 2010 (Joye et al., 2014), as evidenced by oil found on the seafloor below the oiling footprint. Core samples show oil deposition on the seafloor between May and September of 2010, and a 3.8-5 cm "dirty blizzard" layer was found from a core taken in November of 2010 (Joye et al., 2014). In sediment cores affected by the spill, a dark band of fine grained sediment was found in the top 1-2 cm (Hastings et al., 2014). Although the "dirty blizzard" is a likely culprit, this sediment band might also be explained by changes in Mississippi River outflow or by remnants of burnt surface oil (Hastings et al., 2014). Passow et al. reported sinking velocities of marine snow associated with the BP oil)spill to range from 68-553 $m \cdot day^{-1}$, allowing for ~19-2 km-horizontal travel before settling in 1500 m water depth in a 1.0 $cm \cdot s^{-1}$ current of constant direction (Passow et al., 2012).

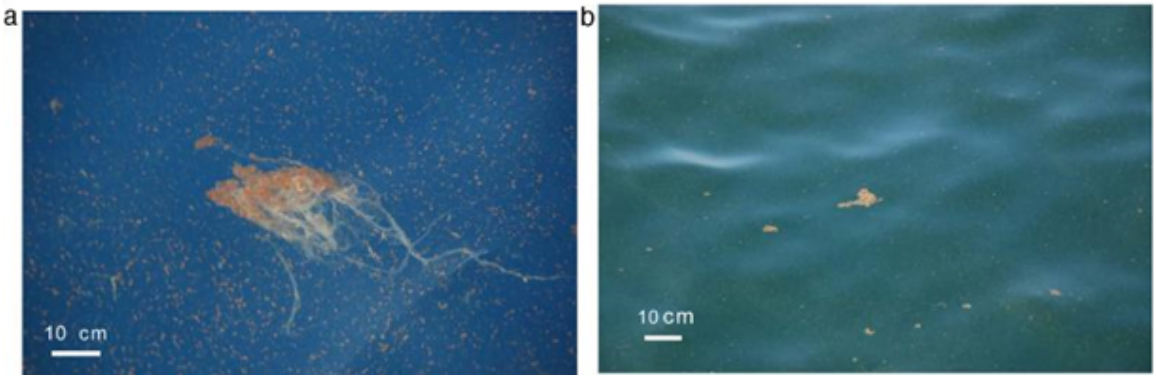

Figure 1. Marine snow aggregates associated with surface slick a) aggregate formed by mucous web b) aggregate formed by oil interaction with suspended matter (Passow et al., 2012). © IOP Publishing Ltd. CC BY-NC-SA

Natural Processes Affecting Marine Snow Bound Spill Oil

Food chain. Processes that degrade marine snow bound oil likely changed as marine snow fell from the surface to depths below the euphotic zone. On a surface exposed to sunlight and turbulence, the oil began the process of weathering. Microbial

oil degraders produce surfactants that emulsify oil (Joye et al., 2014). Emulsification increases bioavailability to other microbial groups (Joye et al., 2014). Bacteria can degrade oil directly as well, by oxidizing, hydrolyzing and assimilating petroleum hydrocarbons (Arnosti, Ziervogel, Yang, & Teske, 2014). Oil aggregates produced in a laboratory using spill oil were associated with alpha- and gammaproteobacterial 16S rRNA gene clones, a deltaproteobacterial clone, and members of *Bacteroidetes* and *Planctomycetes* (Arnosti et al., 2014). Although the extent of microbial degradation is unknown, crude oil degradation is a cooperative biodegradation network, with different bacteria degrading different oil components (Joye et al., 2014). Arnosti et al., 2013 showed distinctive rates and patterns of microbial enzyme activity using oiled aggregates made in a laboratory. In the lab of Arnosti et al., 2013, the polysaccharides pullulan and laminarin underwent hydrolysis in oiled aggregate slurries at rates one or two orders of magnitude higher than in ambient seawater. Rates of pullulan and laminarin hydrolysis were shown to outpace the hydrolysis rates of other polysaccharides by a greater margin in oiled aggregate slurries in comparison to hydrolysis rates in ambient sea water (Arnosti et al., 2014). Arnosti et al., 20143's findings suggested that the enzymatic capability of oiled aggregate communities differed from that of the water column communities. Some oil components were biologically degraded quickly (Joye et al., 2014), but as the oiled particles fell through the water column, biological degradation of the oil could continue. As the oil sank, snow bound bacteria may have continued metabolic processes. Secondary consumers may have degraded intermediates in the oil such as alcohol (Joye et al., 2014). At the seafloor, anaerobic bacteria replaced aerobic ones (Joye et al., 2014). Zooplankton probably ingested oily snow, introducing contaminants into the food chain.

Once in the food chain, oil can be absorbed, adsorbed, ingested, and metabolized (Tansel, 2014).

Settling velocity and biological degradation. The settling velocity of an oiled aggregate would have affected the fate of that oil. Biological activity would have been greater in the mixed layer, and the less time the particle spent in the mixed layer translated into a lower probability of zooplankton ingestion. A rapid fall to the seafloor would have decreased the time aerobic bacteria had to degrade hydrocarbons if the particle fell to an anaerobic seafloor community. Settling velocity is affected by particle density and shape, which also are factors in the ability for a particle to be suspended from the seafloor by bottom currents. Once suspended, a particle may again be exposed to benthic biota that could have degraded or ingested oil in the particle. Slower settling velocity translates into increased time in suspension, allowing more opportunity for benthic interaction.

Vertical Flux

Particle flux described. Settling flux is the particle mass per area within a period of time. This calculation is complicated by differences in particle densities and shapes (Gardner, Southard, & Hollister, 1985), parameters used to calculate mass. Also, particles can change size and density as they collide with other particles, can degrade due to biological activity, and can exchange seawater with denser water. The net vertical flux of particles near the seafloor is the sum of settling particles that are from the surface, settling particles that are from advection, and local particles that have been diffused (Gardner et al., 1985). The vertical flux of particles from the surface is the primary flux. The maximum depth at which primary flux can be measured independently from older material is the clear water minimum (Gardner et al., 1985). Primary flux below the clear

water minimum can be estimated to be the same as above if decomposition and dissolution rates are negligible (Gardner et al., 1985). Decomposition and dissolution rates are less significant for fast settling particles than for slow settling particles. Locally suspended material from the seafloor will diffuse, but flux associated with this diffusion will probably be several orders of magnitude less than settling flux except in cases of high turbulent shear near the bottom (Gardner et al., 1985).

Sediment traps. Sediment traps are an established method of measuring settling flux and determining particle characteristics; however, they introduce uncertainty due to trap induced flow and turbulence (Gardner et al., 1985). Traps deployed below the clear water minimum and above any layer of particles suspended from the local seafloor will trap primary flux particles as well as advection particles that are laterally transported from far away. Traps deployed close enough to the seafloor will trap particles settling out from a locally suspended layer as well.

Suspension and Advection

Suspension and advection described. Marine snow that has reached the bottom can be suspended into the water column with high current velocities (ecogig, n.d.). Once particles reach the seafloor, they are subject to decomposition in the sediments, becoming small enough to suspend (Gardner et al., 1985). Suspension occurs when current induced bottom shear stress exceeds a critical number, and it is influenced by particle size, density, water content, depositional history, and biological disturbance (Laine, Gardner, Richardson, & Kominz, 1994). The time particles stay in suspension is important in terms of transportation, decomposition, and dissolution (Gardner et al., 1985). Having been suspended, particles are susceptible to lateral advection by currents, which is dependent on current velocity and settling velocity. The layer near the seafloor is usually

comprised mostly of suspended particles, the recycling of which allows for dissolution and decomposition before permanent deposition (Gardner et al., 1985). Sediment suspension events may therefore periodically transport oil-remnants from oiled aggregates into the overlying water.

Bottom currents. The dynamic nature of the sediment-seawater interface will cause particles to be transported long distances (Gardner et al., 1985). Bottom currents are likely responsible for the redistribution of seafloor particles from areas of higher bathymetric topography to areas of lower bathymetric topography, such as from the shelf to the slope or from high points on the slope to low points on the slope. As advection forces are generally horizontal due to density stratification, large particles would not be expected to rise in the water column, although Laine et al. (1994) found upslope transport was responsible for deposition of particles on the Bermuda Rise as current velocity decreased over the flat topography of a plateau allowing particles to settle out. Currents that could be transporting particles, and oil associated with particles, may be caused by tidal forcing, storm events, and mid-scale eddies. Tidal currents may be expected to be high frequency, low velocity, and bi-directional. These currents may have a large role in transporting sediment to the slope from the shelf. Mid-scale eddies that break off the Loop Current may provide strong currents that are deeper than tidal currents and more persistent than storm currents. Storm events may have a more extensive reach, providing for episodic advection events throughout the continental margin. Tropical storms may have enough energy to produce currents strong and deep enough to suspend and transport particles at the foot of the slope.

Particle dynamics. Once currents suspend particles, particles settle when gravitational forces overcome vertical and diffusion forces. A sinking particle may be

affected by drag caused by the friction of surface material interacting with a surrounding viscous medium and by the exchange of denser seawater at increased depth. Larger particles generally sink faster than smaller particles even though density may decrease with size (Gardner et al., 1985). Larger particles have less surface area per unit mass and friction on the surface usurps a fraction of gravitational force; however, differing particle forms and densities may have a greater effect on settling velocity than particle size. Depending on the vertical velocity, the particle may have significant horizontal travel with respect to vertical travel. Due to the low excess density of particles, and the amount of time taken for burial, particles may be redistributed many times.

Atlantic studies. Studies of particle suspension and advection on the continental margins of the Atlantic Ocean may have results applicable to understanding the fate of oiled particles that have reached the seafloor of the Gulf of Mexico. In a High-Energy Benthic Boundary Layer Experiments (HEBBLE) project study on the Nova Scotia Rise, it was found that suspension was unlikely with bottom currents below 15.0 $cm \cdot s^{-1}$ (Gardner, Richardson, Hinga, & Biscaye, 1983). In a study of suspension involving current meters, time-series nephelometers, and water samplers on the Bermuda Rise, currents increasing from 3.2 $cm \cdot s^{-1}$ to 9.2 $cm \cdot s^{-1}$ at 31 meters above bottom (mab) were shown to increase particulate matter concentration from 69 $\mu g \cdot l^{-1}$ to 106 $\mu g \cdot l^{-1}$; however, there was a five-day lag between increased velocity and increased particle concentration (Laine et al., 1994). The water depth in this study was 4392 m, tidal variations were found to be moderate, and flux direction was congruent with topographical features (Laine et al., 1994). Currents were found to be faster on the continental slope than on the rise or the abyssal plain, possibly due to obstructions accelerating the regional flow (Laine et al., 1994). Upslope transport, as corroborated by a decrease in water

temperature of 0.1° C, was found to have tripled particle flux with 15.0 $cm \cdot s^{-1}$ currents 31 m above the Bermuda Rise (Laine et al., 1994). Gardner, Southard, and Hollister, 1985 performed a study of the upper rise in the north Atlantic and found evidence of horizontal advection at or possibly above the clear water minimum along continental margins. Once suspended, particles could remain in suspension with less current than was required to pick the particles up from the seafloor (Gardner et al., 1985). Residence time for particles near the seafloor ranged from days for large particles to months for small particles (Gardner et al., 1985). Gardner, Southard, and Hollister (1985) surmised that 50=80% of the material in suspension was in the 20 and 63-micrometer fraction and small particles may have remained in suspension until they dispersed or aggregated into a particle large enough to settle out.

Gulf of Mexico studies. Although Gardner and Walsh, 1990 failed to find a locally suspended layer near the Gulf of Mexico slope seafloor at about 1000 m water depth, large aggregates (>0.5 mm) were found to have been suspended from the seafloor of the slope, probably requiring less bed shear stress to do so than fine grained sediment, and the concentration of large aggregates was about one per liter throughout the water column (Gardner & Walsh, 1990). Near the top of the slope above 400 m water depth, stronger currents may have caused suspension of small and large aggregates, and the continental margin could be the source of a large particle flux to the slope (Gardner & Walsh, 1990). In a study of erosion utilizing sediment cores from a multi corer to study the erosion of the unconsolidated fluffy layer in the Gulf of Mexico, it was found the bottom flow needed for erosion was 28 $cm \cdot s^{-1}$ at MC294, 30 $cm \cdot s^{-1}$ at OC26 and 61 $cm \cdot s^{-1}$ at GC600 (Ziervogel, 2014).

Settling Velocity Equations

Stokes' law. Gardner and Walsh, 1990 used Stokes' law to ascertain settling velocity of marine snow particles in the Gulf of Mexico (Equation 3), resulting in velocities ranging from 45–79 $m \cdot day^{-1}$ (Gardner & Walsh, 1990). Stokes' law assumes that when a spherical particle reaches terminal velocity, frictional force (F_d) is equal to gravitational force (F_g).

$$F_d = 6\pi\mu R v_s$$

Equation 1. Frictional force

μ is dynamic viscosity, R is particle radius, and v_s is settling velocity.

$$F_g = (\rho_p - \rho_f) g \frac{4}{3} \pi R^3$$

Equation 2. Gravitational force

ρ_p is particle density, ρ_f is seawater density, and g is gravitational acceleration. Other assumptions are: laminar flow, homogenous material, smooth surfaces, and no particle interference. Stokes' law is to be used with low Reynolds numbers. Reynolds numbers are ratios of inertial forces to viscous forces (Falkovich, 2011), and Reynolds numbers of 10 or less are associated with laminar flow in the case of a sphere in a fluid for which Stokes' law can be applied. Velocity (v_s) is found by solving Equation 3.

$$v_s = \frac{2}{9}\frac{(\rho_p - \rho_f)}{\mu} gR^2$$

Equation 3. Stokes' law

The use of Stokes' law to determine marine snow settling velocity is problematic due to the inherit assumptions. Marine snow particles are rarely spherical, and deviations from a sphere may increase form drag in the case of protrusions that increase surface area. Aggregated material on the particle surface may reduce laminar flow. Marine snow particles are not homogenous with respect to heavier than water materials, as Passow et al. found water in marine snow from the oil spill to account for 99.7% of particle volume (Passow et al., 2012). Particle surfaces may be comprised of smaller aggregates that agglutinate after particle collisions, as particle interference probably occurs throughout the water column.

Ploug, Terbruggen, Kaufmann, Wolf-Gladrow, and Passow (2010). Ploug et al. (2010) incorporated a calculation for Reynolds number (Re) in their drag coefficient (C_D) to develop another equation used to calculate particle settling velocity (v_s).

$$Re = \frac{dv_s}{\nu}$$

Equation 4. Reynolds number

d is particle diameter, and ν is kinematic viscosity.

$$C_D = \frac{24}{Re} + \frac{6}{1 + \sqrt{Re}} + 0.4$$

Equation 5. Drag coefficient

$$v_s = \left(\frac{2g\Delta\rho V}{\rho_f C_D A}\right)^{0.5}$$

Equation 6. Settling velocity (Ploug et al., 2010)

Δρ is aggregate excess density, V is particle volume, and A is aggregate cross-sectional area.

Study Sites

OC26

Description. OC26 (28˚ 44.20' N, 88˚ 23.23' W) is located in the Mississippi Canyon lease block 297 (MC297) 3.5 km to the south of the Deepwater Horizon well site. It is about 80 km south-east of the Mississippi River mouth. Named after a visit by RV Oceanus in 2010, OC26 was chosen as a research site by the Ecosystem Impacts of Oil and Gas Inputs to the Gulf (ECOGIG) consortium, one of eight consortia funded through the Gulf of Mexico Research Initiative (GOMRI) (Diercks et al., 2013.). It is situated downslope of the continental shelf and in areas of abrupt changes in seafloor elevation, having a depth of about 1500 m (Figure 2). To the East of OC26 lies a large bathymetric feature called Gloria Dome (Diercks et al., 2013).

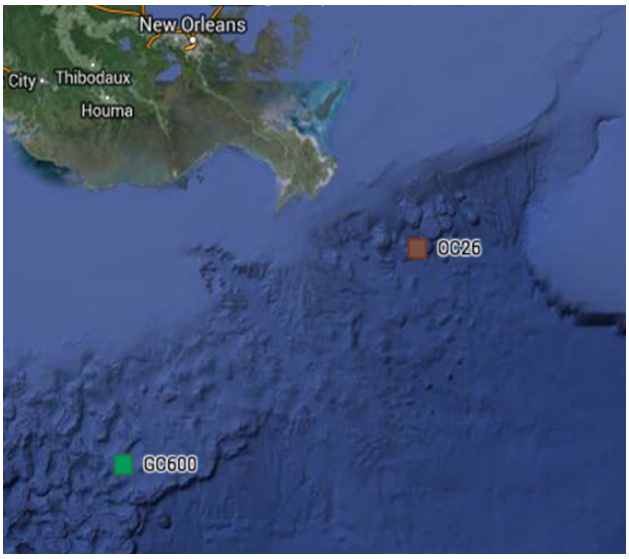

Figure 2. OC26 and GC600

Hurricane Isaac. Hurricane Isaac made landfall on the Louisiana coast near the mouth of the Mississippi River on August 29th, 2012 00: 00 UTC (Berg, 2013) (Figure 3). The slow moving storm produced tropical force winds for up to 45 hours and heavy rainfall. On August 28th, 2012 1800 UTC, the storm had wind speeds of 70 kts and was located 43 km from OC26 (Berg, 2013) (Figure 3).

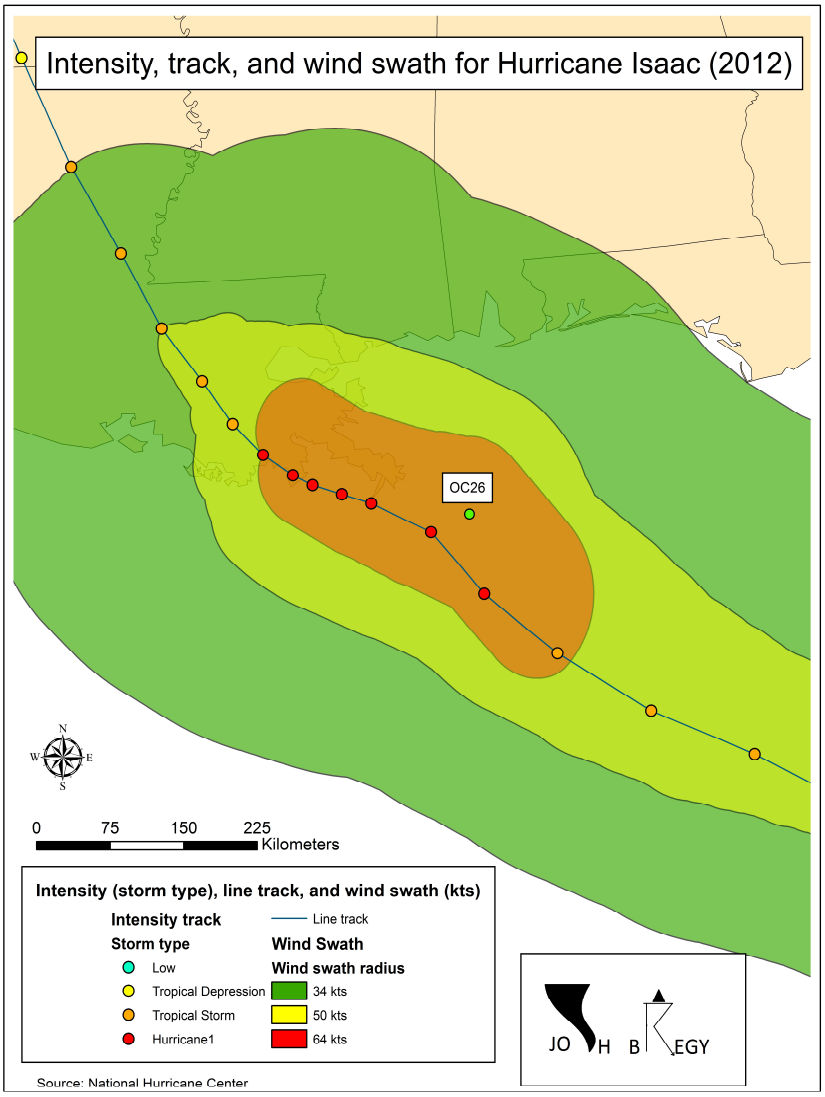

Figure 3. Intensity, track, and wind swath for Hurricane Isaac (2012) Storm type depicted by orange (Tropical Storm) and red (Hurricane1) circles. Wind swath is depicted by reddish (64 kts), yellowish (50 kts), and green (34 kts) fields (figure by Josh Bregy, used with permission).

Figure 4. Observed footprint of BP oil (SkyTruth)

Hydrocarbons. OC26 was in the oiling footprint (Figure 4). Deleterious effects of oil have been found in a study of coral at this site, indicating that oil reached the sea floor (Fisher et al., 2014). The coral in this study exhibited dead or hydroid-covered colonies that retained small branches, indicating recent impact with respect to November of 2011 (Fisher et al., 2014). The damage was patchy across the site, suggesting effects of contaminating micro droplets or particles (Fisher et al., 2014). A study of core samples from Mississippi Canyon 294, located 11 km to the southwest of the site of the *Deepwater Horizon* well site discovered the presence of oil in the top two centimeters of sediment (White et al., 2014). Within eight core samples taken in December 2010, a range of 32–9300 $\mu g \cdot g^{-1}$ of oil was present (White et al., 2014). Natural gas seeps were found at this site in 2011 by the NOAA ship Okeanos explorer (Diercks et al., 2013). Reservoirs of hydrocarbons are a source of not only low-molecular-weight gases such as methane, ethane, propane, butane, and pentane in differing proportions but also of crude oil (Joye et al., 2014).

GC600

Description. GC600 is located to the southwest of and a bit shallower (~1390 m) than OC26. It is located about 285 km from the well site, within the Green Canyon lease area (Passow et al., n.d.).

Hydrocarbons. GC600 was away from the oil footprint (Figure 4). Surface slicks from natural hydrocarbon seepage have been observed at GC600. This site is home to "Oil Mountain", an area of prolific natural seepage characterized by seafloor gas hydrate deposits (Hu, Yvon-Lewis, Kessler, & MacDonald, 2012). Bacterial metabolism of the hydrocarbons utilizes oxygen, but sulfate and carbon dioxide are also scavenged for oxygen. Bacteria at the seep secrete calcium carbonate forming a hard substrate much

like a coral reef. A community indigenous to the seep is comprised of corals, tubeworms, clams, mussels, and crabs.

Hypotheses

First Hypothesis

Density increase with oil degradation. As buoyant surface oil was observed in marine snow aggregates that formed and later sank in the area of the spill site, remnants of this oil may still be in the flocculent layer beneath the spill site. Because the surface oil was buoyant, rising from about 1500 m water depth, the components of the marine snow that incorporated and sank this oil must have been dense enough to overcome the buoyancy of slick oil, the later degradation of which may have caused the marine snow settling velocity to increase. Crude oil is comprised of a mixture of saturated and aromatic hydrocarbons, resins, and residue (Joye et al., 2014). Within the aggregates, it is possible that components such as polycyclic aromatic hydrocarbons and residue cannot be assimilated by bacteria as light and labile components can. Thus the particle density, hence the settling velocity, of the host aggregate may have increased since settling from the surface. Marine snow that has settled from the oiling footprint may now have higher excess densities and settling velocities than non-oiled marine snow. Marine snow particles settling near the seafloor at OC26 are hypothesized to have faster settling velocities than particles settling near the seafloor at GC600.

Second Hypothesis

Settling marine snow periodicities. As local suspension is only one of three expected contributors of particles to the mooring sites at both OC26 and GC600, any periodicity in the resettling of locally suspended particles may not reflect the overall

periodicity of settling particles. Advection and primary fluxes may contribute a relatively large number of particles to the mooring sites. Given the location of the two sites in the continental margin, both biological activity in surface waters and lateral transport of seafloor sediment are expected to be particle sources of import. As particles from the shelf move towards the study sites, they may separate vertically due to settling velocity differences and laterally due to current velocity differences, effectively "washing out" a periodicity settling signal.

"Washing out" local suspension signal. Particles that are locally suspended on the seafloor may resettle in "waves" that are separated by settling velocity. These "waves" of settling particles would vertically diverge as vertical advection forces relaxed. Allowed to settle while unaffected by advection forces, pulses of settling material would settle that reflected the periodicity of the suspending currents. The pulses would lag behind the current reflecting particle settling velocities and distances. However, during quiescent periods between suspending currents, particles that have been laterally transferred or have been falling from the euphotic zone would have a chance to settle, and their settlement periodicity may reflect periods of advection currents or of primary production. Settling periodicity of locally suspended particles would be "washed out" by the periodicity of the two other particle sources. For the data from the study sites, power spectra of particle concentrations are not expected to have the same peaks as power spectra of current velocities.

CHAPTER II

MATERIALS AND METHODS

Instruments

Marine Snow Cameras

Design. To characterize the settling velocity of marine snow near the bottom of the water column at OC26 and GC600, two marine snow cameras were built and deployed on moorings (Figure 5). Both cameras were similar in design and were enclosed with an aluminum pipe cage that was 91 cm tall, 61 cm wide and 91 cm long. Within each cage, a 20.32 cm by 20.32 cm by 20.32 cm clear acrylic viewing chamber was fastened, having a volume of ~8.4 L (Figure 6). The viewing chambers were sealed to prevent sample from escaping, but from the top of each chamber a 122 cm PVC pipe that was 10.16 cm in diameter stilling chimney was attached so that particles could enter the chamber. The cylinders formed by the areas of the stilling chimney openings and the heights of the boxes were about 1.65 L. Due to density concerns, there was no poison added to the viewing chambers, so biotic degradation could have been significant over the deployment durations, which ranged from 3 to 11 months. A Nikon D7000 camera encased in an HBR-1600 pressure housing rated for 6000 m was secured at an optimal focal distance from each chamber. The camera deployed at OC26 utilized a 20 mm lens, whereas the camera at GC600 was fitted with a 35 mm lens for optimal optics. The 20 mm lens had a focus distance setting of 0.3 m, whereas the 35 mm lens had a focus distance setting of 0.45 m, allowing for less apparent size differences in similar objects on either side of the focal points, the centers of the viewing chambers. The front of the pressure housing with the 20 mm lens was positioned 19 cm from the focal point, and the front of the pressure housing with the 35 mm lens was positioned 28 cm from the focal

point. The camera settings for the Nikon D7000s were: f-stop f/22, exposure time 1/60 s, and ISO speed ISO-100. Strobes were mounted orthogonally to the camera-viewing chamber lines to illuminate particles, lighting the entire volume of the boxes.

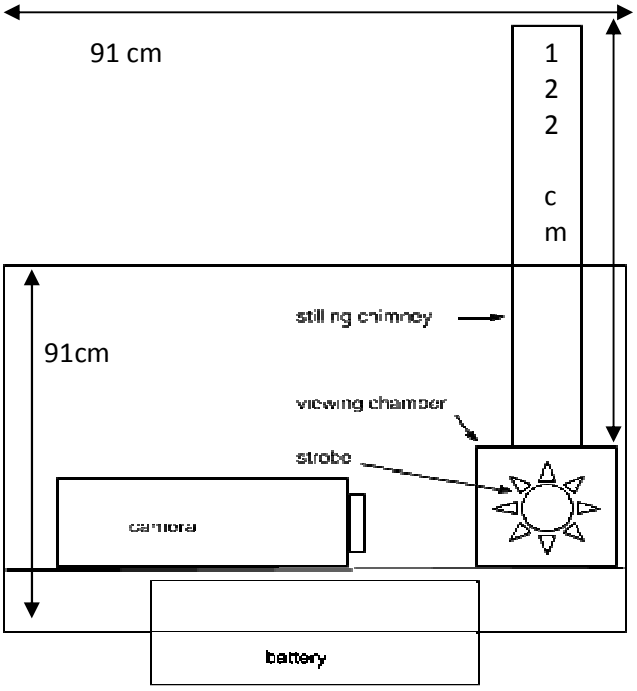

Figure 5. Marine snow camera

Collection method. At the time of the sampling, suspended sediments may have contained particulate material from the oil-fallout of the Deepwater Horizon spill in 2010. The stilling tubes that feed the viewing chambers protrude above the frames of the marine snow cameras but not above the bridles used to attach the marine snow cameras to the moorings. Particles entering the tube on their original trajectory would be free of current effects and gravitationally settle to the bottom of the viewing chamber. The collection method may prevent long particles from entering the stilling chimney at high lateral current velocity. For example a particle settling at 100 $m \cdot day^{-1}$ in a 10.0 $cm \cdot s^{-1}$ lateral current would have a vertical travel of about 1.2 mm in 10.16 cm (the diameter of chimney) of horizontal travel, thus longer particles may catch on the edge of the chimney

opening and either settle into the chamber as fragments or not enter at all. Suspended particles also would not be expected to enter the viewing chamber. The sampling bias was acceptable as the purpose of the experiment was to compare densities of similar sized particles, and elongate particles entering the box would be problematic with the spherical particle assumption of Equation 3, while suspended particles may be smaller than the 0.5 mm diameter definition of marine snow. Having reached terminal velocity by the time they entered the viewing chamber, particles could have been anywhere in the cylinder of the stilling chimney, and particles of the same size would appear smaller in images if they were farther from the camera. The distance from the camera probably averaged out over time.

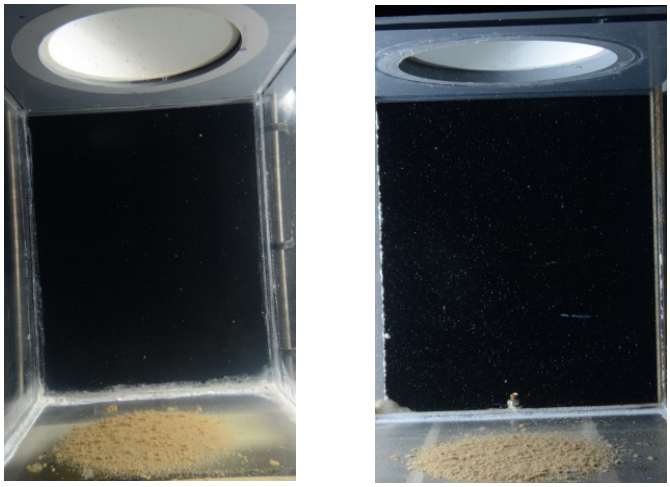

Figure 6: Viewing chambers A) OC26 (20 mm lens) B) GC600 (35 mm lens)

Camera timing. The HBR-1600s were equipped with interval meters to control the timing of the cameras. As the deployments spanned several months, images were taken in bursts every hour or other hour followed by a shutdown of the system to conserve battery and memory. The image intervals were used so that an individual particle would be imaged multiple times as it settled in the viewing chamber (Figure 6). Upon the first turnaround of the camera at OC26, many particles were observed to have

settled faster than the initial interval would allow for subsequent imaging. Slow settling particles were tracked across several images, and no acceleration was observed, thus the interval meters were reconfigured to allow shorter intervals. The new configuration was used on the third OC26 deployment and the second GC600 deployment. Images from the third deployment at OC26 and the second and third deployments at GC600 have not been analyzed and no data from these deployments have been used.

Table 2

Image Intervals

	Dates (mm/yy)	Site	Interval (s)
1.	06/12-09/12	OC26	60|60|120|240|3120
2.	09/12-10/13	OC26	60|60|60|60|120|240|480|6120
3.	09/14-	OC26	20|20|20|20|20|20|20|7060
4.	09/12-06/13	GC600	60|60|120|120|240|3000
5.	06/13-05/14	GC600	20|20|20|20|20|20|20|7060
6.	05/14-	GC600	20|20|20|20|20|20|20|7060

Moorings

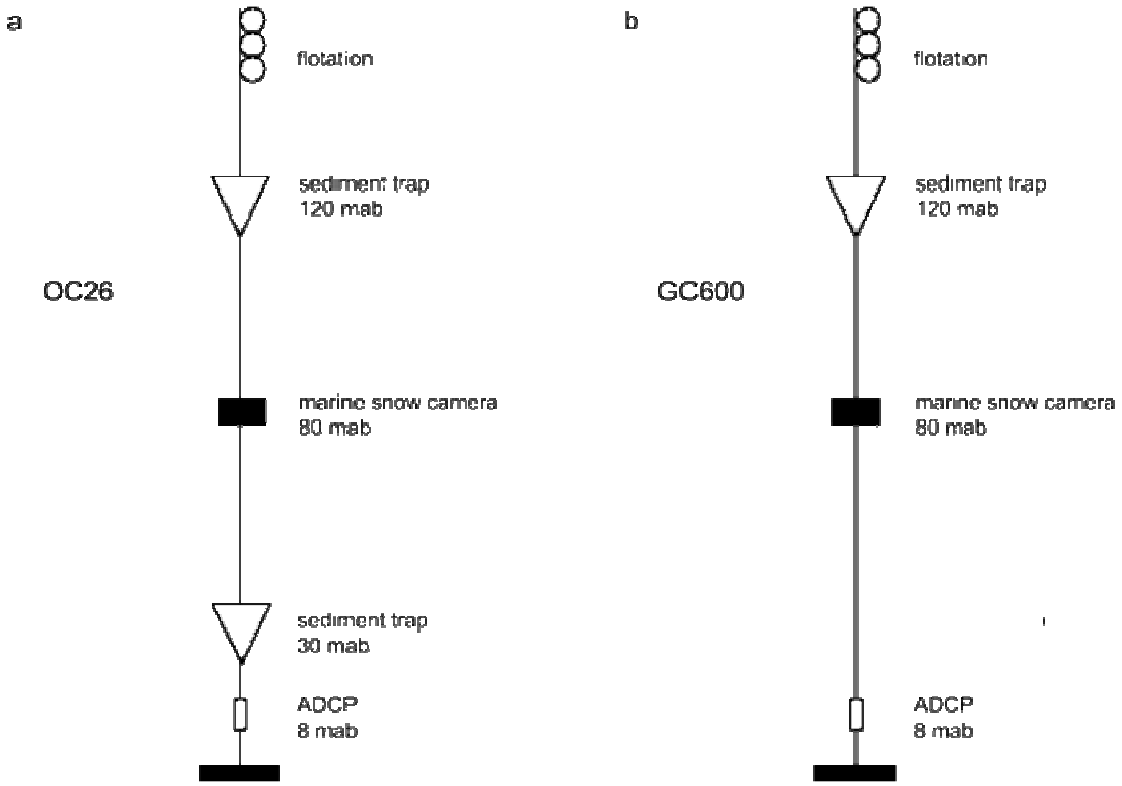

Figure 7. Moorings a) OC26 b) GC600

Moorings. The marine snow cameras were deployed with moorings hosting sediment traps and Acoustic Doppler Current Profilers (ADCPs). The mooring deployed at OC26 included sediment traps manufactured by McLane fastened at 120 mab to capture fallout from distant advection and at 30 mab to capture fallout from local suspension (Figure 7). The mooring at GC600 included a sediment trap manufactured by McLane fastened at 120mab (Figure 7). The sediment trap intervals were set at 18 days for all deployments at both sites except the third deployment at OC26. The second deployment at OC26 resulted in a failure of the bottom sediment trap, so only the top trap was redeployed and an osmotic sampler was put where the bottom trap was. For the third deployment at OC26, the McLane trap was programmed to have about 17 day intervals.

Along with material transported from the seafloor, primary flux may be captured in all the traps. The RDI ADCPs were 300 kHz and sampled hourly.

Water Column Profiles

Marine snow profiles. In the vicinity of OC26, three vertical water column profiles of suspended particles were obtained during three nighttime deployments of a combined camera-CTD system mounted onto a metal frame called a Marine Snow Camera (MSC), showing number of particles in the water column. Images of a volume of seawater defined by a collimated strobe flash were taken at 10 s intervals as the MSC was lowered, providing an image for roughly every meter of the water column. Each image was assigned a depth. The images were analyzed using Image-Pro software; visual particles >0.5 mm were counted and are reported as aggregates L^{-1}. The following parameters of each particle were quantified: area, aspect ratio, major axis, minor axis, maximum diameter, minimum diameter, mean diameter, perimeter, length, and width. The particle parameters were divided into ten intervals, and the number of particles per liter in each interval was calculated. Cast #3, taken September 9, 2012, went down to 1472 m. There was spill oil on the surface when this cast was done. Cast #4, taken September 13, 2012, went down to 1454 m. Cast #5, taken September 14, 2012, went down to 1465 m.

Figure 8. Marine snow profile locations near OC26 The red line represents about 5 km.

Analyses

Settling Velocities

Parameters. The images from the marine snow cameras were processed using Image-Pro Plus software. A calibration file was created for each deployment, and the individual images were sequenced in bursts. The number of marine snow particles per image and time of the image were recorded. Area, center-X, center-Y, angle, diameter (mean), and roundness were recorded for each marine snow particle imaged. Area was the cross sectional area of the particle, center-X was the X coordinate of the image that gave the vertical position of the particle in the viewing chamber, center-Y was the Y coordinate of the image that gave the horizontal position of the particle in the viewing chamber (when analyzed, the images were oriented with the image tops and bottoms parallel to the settling paths), angle was the angle of orientation of the particle, diameter

(mean) was the mean diameter of the particle, and roundness was calculated using Equation 7.

$$roundness = \frac{perimeter}{4\pi * area}$$

Equation 7. Roundness

Settling velocity calculations. A particle tracking program was developed and used to determine the settling velocities of all settling particles found in at least two consecutive images, using 0.5 mm diameter (mean) as a lower bound. The same particle in consecutive images was found by comparison of parameters. Time between images was established by the interval meter and was read from image timestamps. As particles had been assigned coordinates in pixels, the difference in coordinate vectors assigned to the same particle in consecutive images was converted to millimeters using a conversion factor from calibration files. Assuming gravity and friction to be the only acting forces, particle settling velocities could then be calculated. The parameter magnitudes (excepting center-X), plus or minus the following increments, were compared to the parameter magnitudes of other particles in the subsequent and/or consecutive images: area +/-0.25 mm^2, center-Y +/-10 mm, angle +/-90°, diameter +/-0.5 mm, and roundness +/-1. If the magnitudes of the parameters above did not match parameter magnitudes of a particle in subsequent or consecutive images considering the increments, the particle was assigned a minimum settling velocity. If a particle were in the first image of a sequence and not in the second image, the minimum velocity was the distance travelled to the bottom of the image per minute. If the particle was in an image in the middle of the sequence and could not be found in the image before or after, the distances travelled from the top and to the bottom were divided by the interval of the particle's image and the next

image, respectively, and the largest resulting settling velocity was assigned as the particle's minimum settling velocity. A particle found in the last image of the sequence not found in the penultimate image was assigned a minimum settling velocity of the distance the particle had fallen divided by the interval between the two images.

Densities

Back calculations. With settling velocities and sizes known, densities were back calculated from the settling velocity equations (Equation 3 and Equation 6). The values used for Equations 3 and 4 (Stokes' law and Reynolds number) are tabled below (Table 3). Equation 3 (Stokes' law) utilized the constants of ρ_f (seawater density), μ (dynamic viscosity), and g (gravitational acceleration). Equation 4 (Reynolds number) utilized the constant ν (kinematic viscosity). Reynolds number was used in Equation 5 to calculate a drag coefficient for Equation 6 (Ploug et al., 2010).

Table 3

Parameters for Equations 3 and 4

Equation	ρ_f ($g \cdot mm^{-3}$)	μ ($Pa \cdot s$)	g ($mm \cdot s^{-2}$)	ν ($mm^2 \cdot s^{-1}$)
1. Equation 3	1.027E-03	1.88E-03	9.8E03	
2. Equation 4				1.83

ADCP Data Analyses

Power spectral density plots. Power spectral density plots (PSDs) were created for current velocity (east, north, vertical, and magnitude) as well as for temperature and depth data from the ADCPs. A Hann window of 720 hours (about one month) with a 90% overlap was used. The coefficients of a Hann window are calculated using Equation 8.

$$w(n) = 0.5\left(1 - \cos\left(2\pi\frac{n}{N-1}\right)\right), 0 \le n \le N$$

Equation 8. Coefficients of a Hann window

w(n) returns the coefficients of a Hann window and the window length (L) =N+1.

Analysis of ADCP data affected by Hurricane Isaac. The OC26 current data contained signals from an apparent storm event at the end of August 2012, and ADCP series and ancillary data spanning mid-August through the mooring turnaround on September 9 were plotted in order to examine storm effects at depth.

Bihourly Particle Counts

Instantaneous counts. Data from the first image of a sequence taken every other hour, or bihourly, was used to record instantaneous particle counts and average particle areas of particles settling in the viewing chambers. Only the first image of every bihourly sequence was used to ensure particles were not counted twice and to compare datasets between OC26 and GC600, as the GC600 interval meter commanded bihourly sequences. Average ESDs were calculated from average particle areas and, subsequently, average aggregate volumes were calculated. Dates with times were assigned to the data. Volumes were assigned to viewing areas in the images, considering the stilling chimney areas and the heights of the analyzed part of the viewing chambers. Particle counts were then used to calculate particle concentrations. A time series of particle counts, concentrations, and aggregate volume concentrations were developed and compared. Power spectral densities were generated for the particle concentrations and volume concentrations in order to examine signals that may relate to current periods. Hann windows of 720 hours (about one month) with a 90% overlap were used. Hann windows

were used to accentuate frequencies of less than one month. The coefficients of the Hann windows were calculated using Equation 8.

CHAPTER III

RESULTS

Particle Size and Settling Velocity

Settling Velocities and Diameters (Mean)

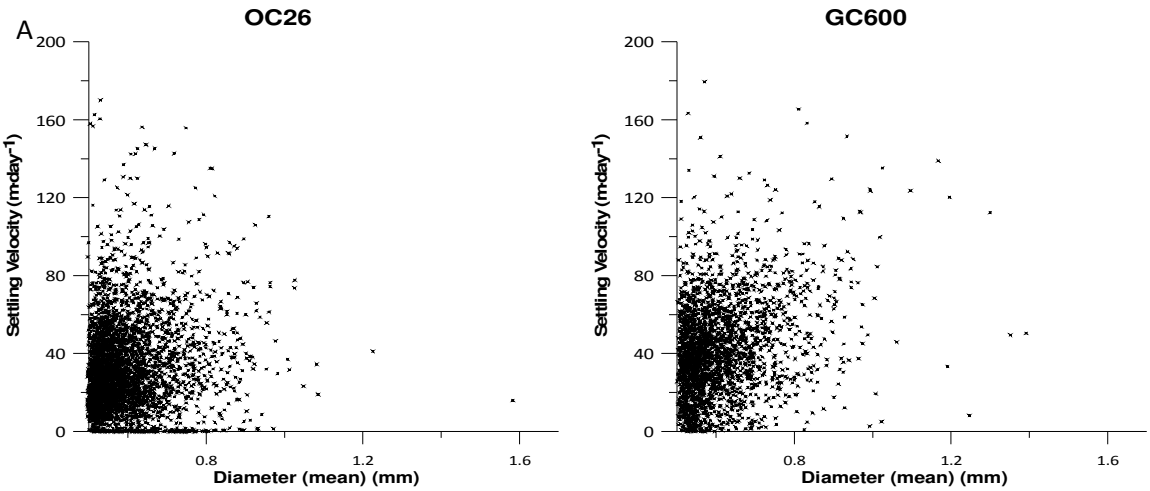

Figure 9. Settling velocities vs diameters (mean) A) OC26 B) GC600

Averages. Settling velocities were plotted against diameters (mean) at both sites (Figure 9). Settling velocities and diameters (mean) were obtained for 3,611 particles at OC26 from June 26, 2012 1:00 PM–February 17, 2013 1:24 PM, an average of about 0.64 particles per hour. The average velocity was 32.4±22.7 m·day^{-1} and the average diameter (mean) was 0.59±0.09 mm (Table 4). At GC600, settling velocities were assigned to 2430 particles from September 8, 2012 12:00 PM-December 28, 2012 3:24 PM, an average of about 0.91 particles per hour. The average velocity was 42.3±24.3 m·day^{-1} and the average diameter (mean) was 0.61±0.10 mm (Table 4). Sequences from the marine snow cameras overlapped from September 11, 2012–December 27, 2012, for which time settling velocities and diameters (mean) were assigned to 1,435 particles from OC26 and 2,335 particles from GC600. Of these particles, the average diameter (mean) and settling velocity at OC26 was 0.59±0.09 mm and 30±20 m·day^{-1}, and the average

diameter (mean) and settling velocity at GC600 was 0.6±0.1 mm and 40±20 m·day^{-1} (Table 4).

Table 4

Average Diameters (mean) and Settling Velocities Found at OC26 and GC600

Site	Average Settling Velocity	Average Diameter (mean)
OC26 (total)	32.4±22.7m·day^{-1}	0.59±0.09mm
GC600 (total)	42.3±24.3m·day^{-1}	0.61±0.10mm
OC26 (contemporary)	30±20m·day^{-1}	0.59±0.09mm
GC600 (contemporary)	40±20m·day^{-1}	0.6±0.1mm

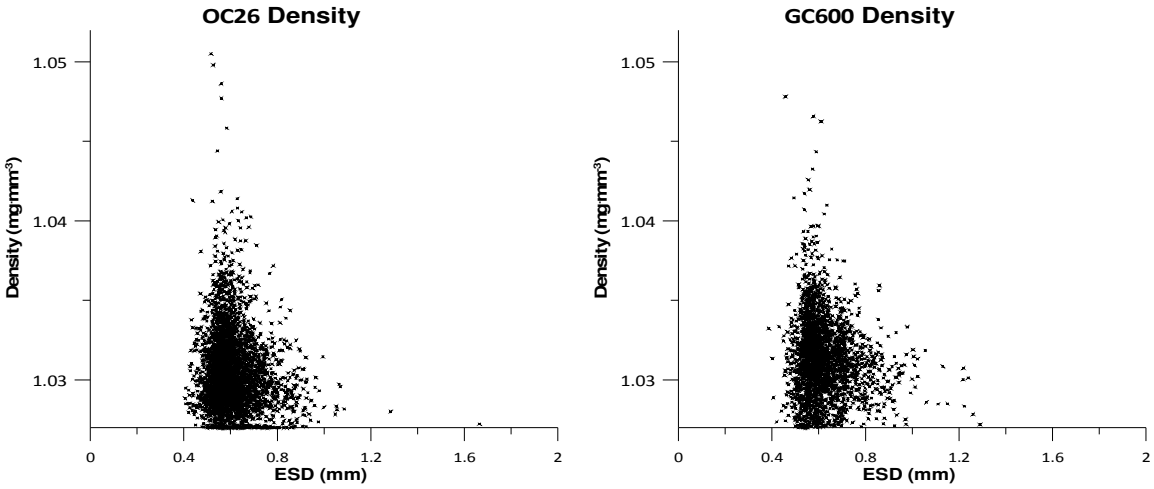

Figure 10. Density vs ESD A) OC26 B) GC600

Time Series Analyses

ADCP Data

Averages. The average current velocity (magnitude) at OC26 was less than that of GC600 during the first respective deployments (06/12-09/12 at OC26 and 09/12-06/13 at GC600), as the average at OC26 was 4.2 cm·s^{-1} and the average for GC600 was 5.1

$cm \cdot s^{-1}$ (Figure 11 and Figure 12). However, OC26 experienced two episodes of relatively high current velocity (magnitude), with speeds above 12.5 $cm \cdot s^{-1}$, during the first deployment (Figure 11). The first period of high current velocity was immediately following the deployment and the other period was during the late summer (Figure 11). Current velocities (east and north) were averaged for both sites (Figure 11 and Figure 12). The average current near the seafloor at OC26 during the time of the first deployment was to the north at over 1 $cm \cdot s^{-1}$ (Figure 11). The average current near the seafloor at GC600 during the time of the first deployment was easterly at over 1 $cm \cdot s^{-1}$ (Figure 12). Hurricane Isaac passed near OC26 in late August, and current effects were recorded by the ADCP (Figure 13).

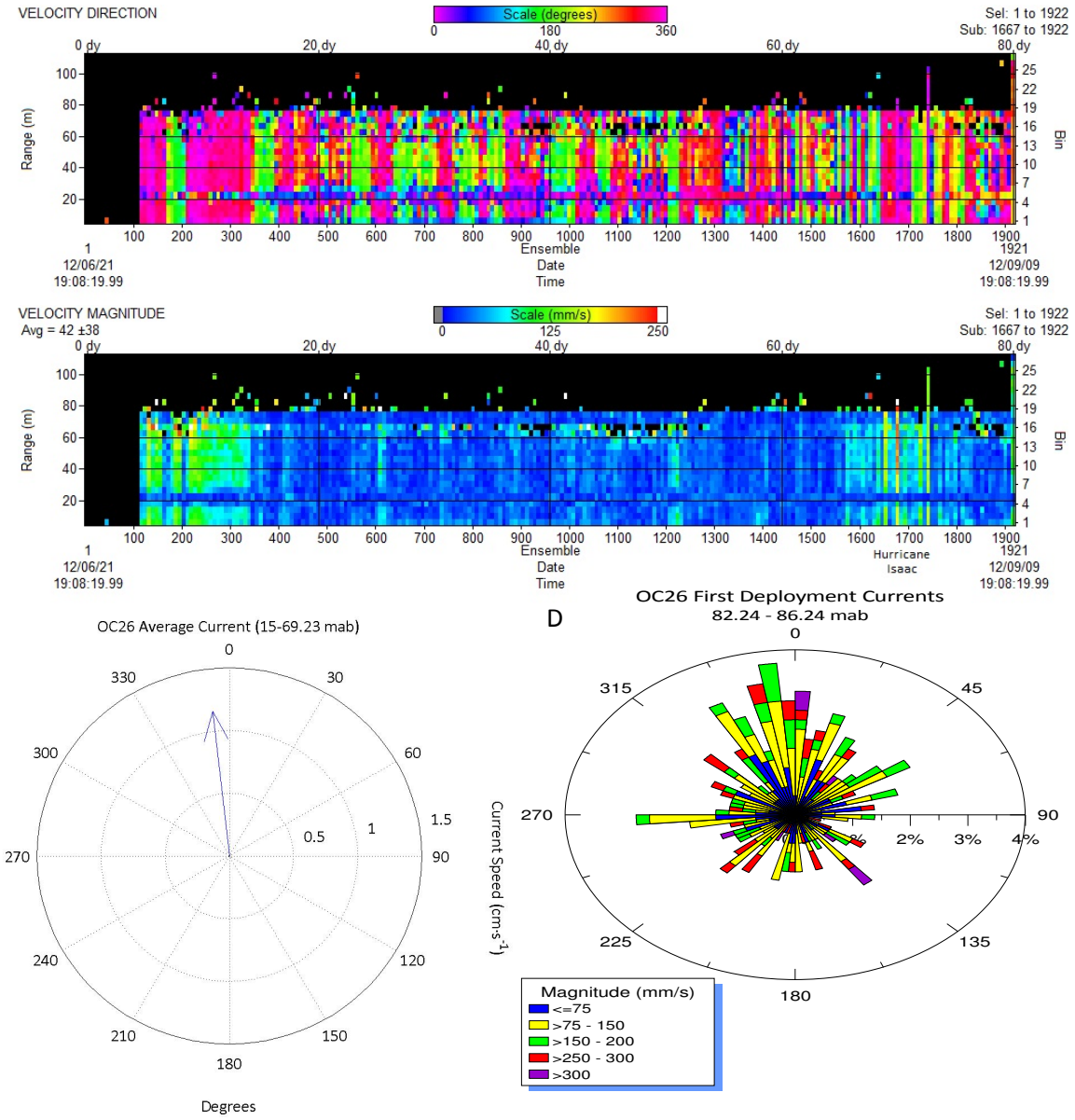

Figure 11. OC26 current velocity A) direction current is flowing to B) magnitude C) average current velocity D) direction of current and frequency of magnitude with respect to direction For direction, purple represents currents flowing to the north and green represents currents flowing to the south, and for magnitude, blue represents 0 mm·s^{-1} and red represents 250 mm·s^{-1}. The percentage of velocity magnitude for each direction is also shown where blue represents currents equal to or less than 75 mm·s^{-1} and purple represents currents greater than 300 mm·s^{-1}.

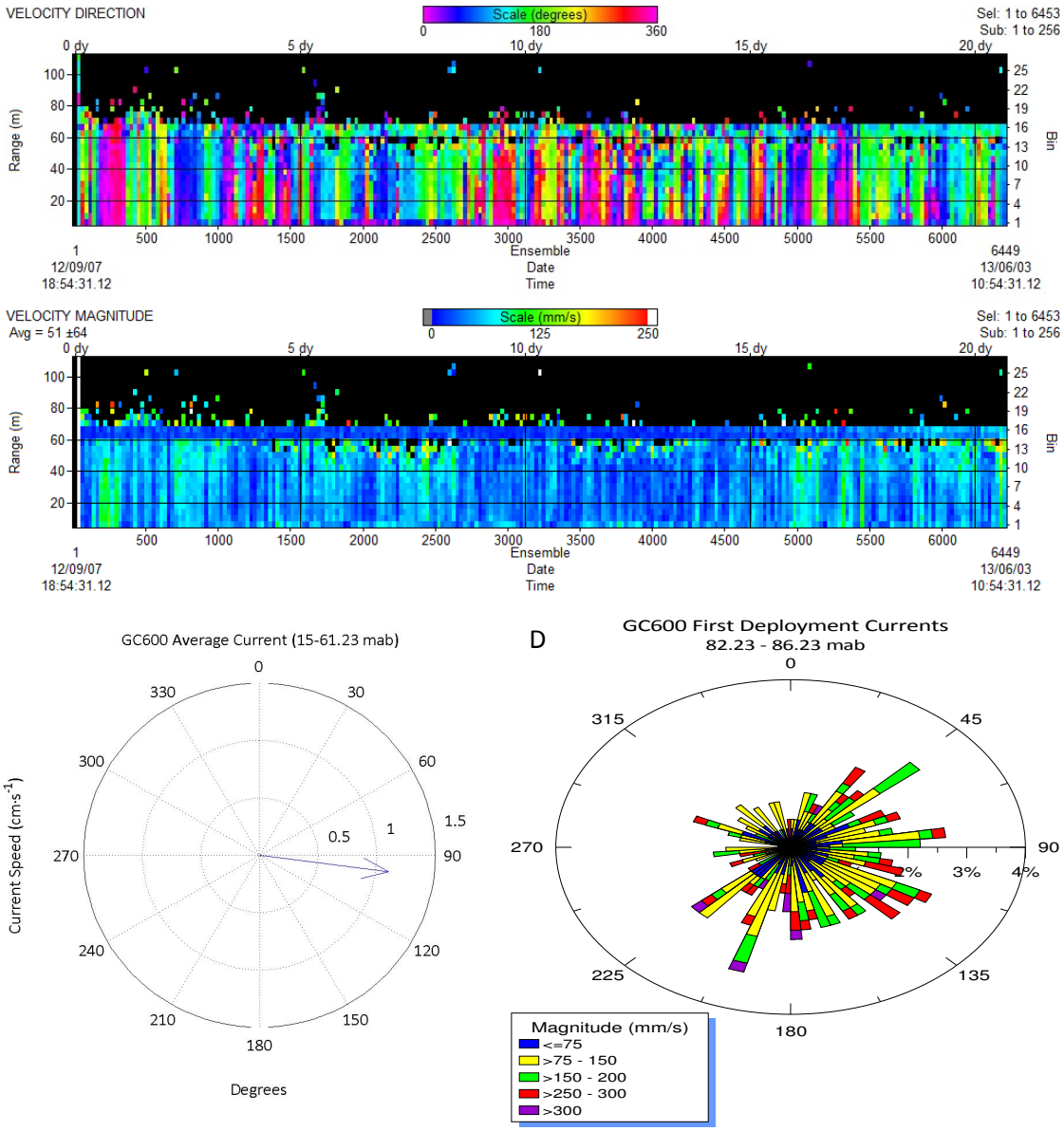

Figure 12. GC600 current velocity A) direction current is flowing to B) magnitude C) average of current velocity D) direction of current and frequency of magnitude with respect to direction For direction, purple represents currents flowing to the north and green represents currents flowing to the south, and for magnitude, blue represents 0 $mm{\cdot}s^{-1}$ and red represents 250 $mm{\cdot}s^{-1}$. The percentage of velocity magnitude for each direction is also shown where blue represents currents equal to or less than 75 $mm{\cdot}s^{-1}$ and purple represents currents greater than 300 $mm{\cdot}s^{-1}$.

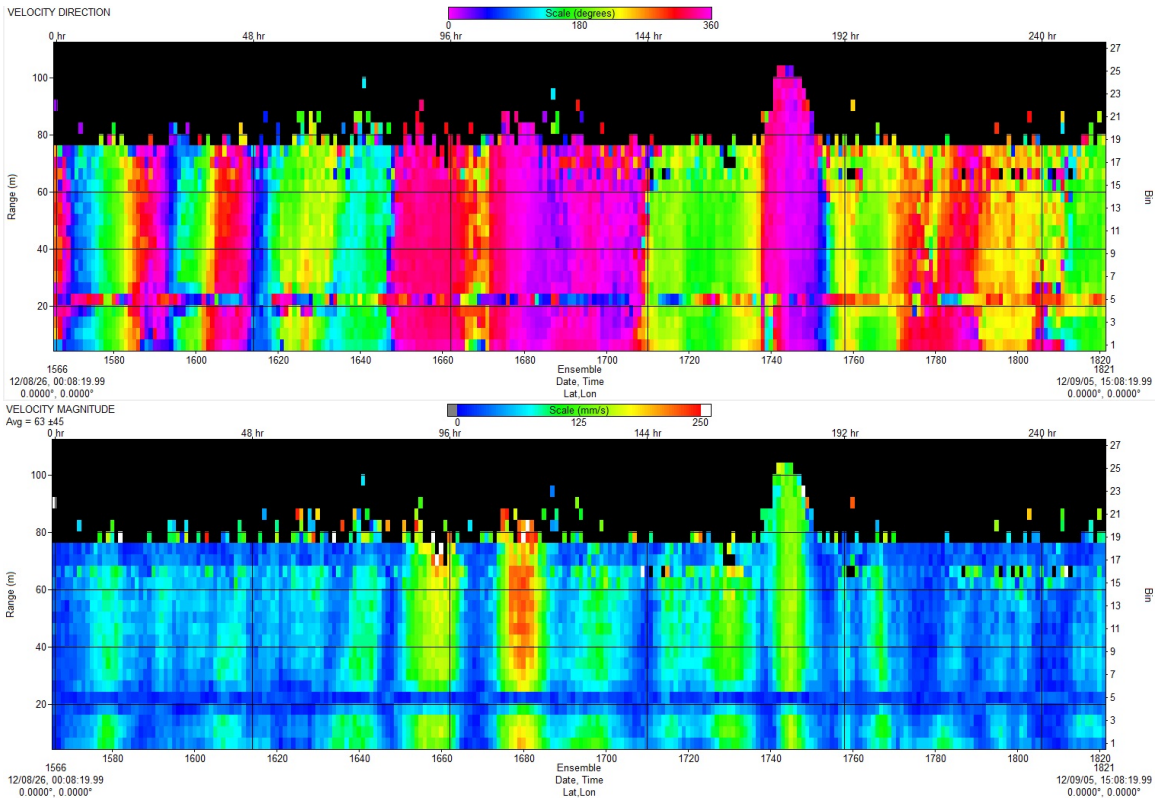

Figure 13. OC26 current velocity A) direction B) magnitude For direction, purple represents currents flowing to the north and green represents currents flowing to the south, and for magnitude, blue represents 0 mm·s^{-1} and red represents 250 mm·s^{-1}.

Periodicities. The data from the first bin of the series data (current speeds) and from the ancillary data (temperature and depth) were used to plot Welch's overlapped segment averaging (WOSA) estimates (Figure 14-Figure 17). The first bin of the series data encompassed 15-21.23 mab and the ancillary data was from 8 mab. Hann windows of 720 hours and 90% overlap were used to accentuate signals of less than a month in period. The broken lines on the plot insets outline the 95% confidence interval. A peak in current velocity (east) at OC26 is seen at 21.79 hours (Figure 14). This peak is also seen in current velocity (north), but the most pronounced peak in the current velocity (north) estimate is at 73.14 hours (3.0475 days) (Figure 14). This pronounced peak of 73.14 hours (3.0475 days) in the current velocity (north) estimate is observed in the temperature estimate as well (Figure 14 and Figure 15). There is a split peak in the OC26

depth estimate at 23.81 and 25.6 hours, of which the former peak can be seen in the temperature estimate also (Figure 15). At GC600, there is a peak at 12.34 hours and there is also a peak at 21.79 hours in the current velocity (east) estimate (Figure 16). A split peak of 21.79 and 23.81 hours is seen in the current velocity (north) estimate (Figure 16). This split peak may explain the 22.26 hour peak vice 21.79 hour peak shown in the current velocity (magnitude) estimate (Figure 17). A pronounced 23.81 hour peak is seen in the GC600 depth estimate, which is actually a split peak with 25.6 hours as seen at OC26 (Figure 17). A 73.14 hour (3.0475 day) peak is seen in the GC600 temperature estimate as seen at OC26, along with a 21.79 hour peak (Figure 17).

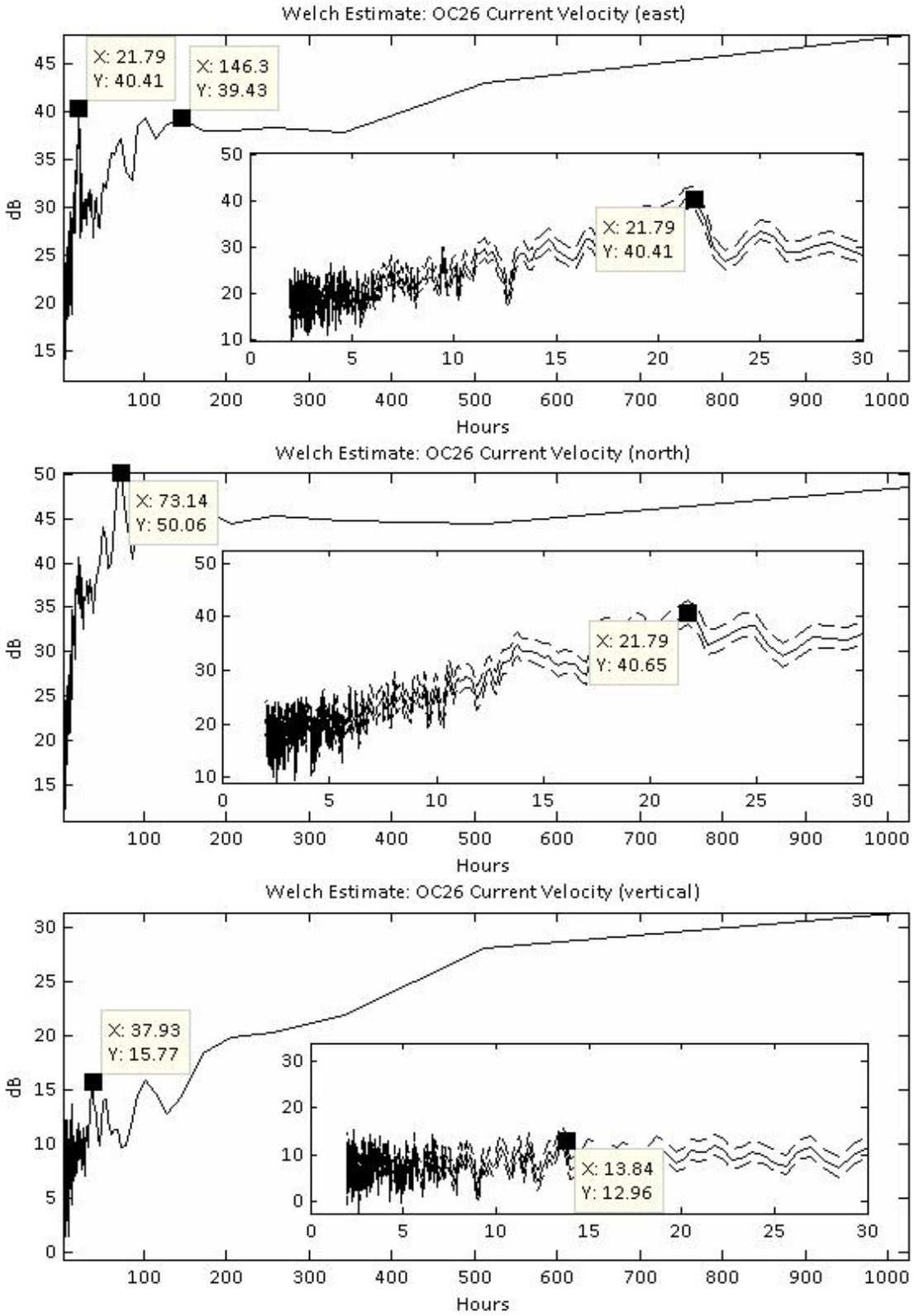

Figure 14. OC26 WOSA spectral estimations A) current velocity (east) B) current velocity (north) C) current velocity (vertical) The broken line in the inset represents a 95% confidence interval.

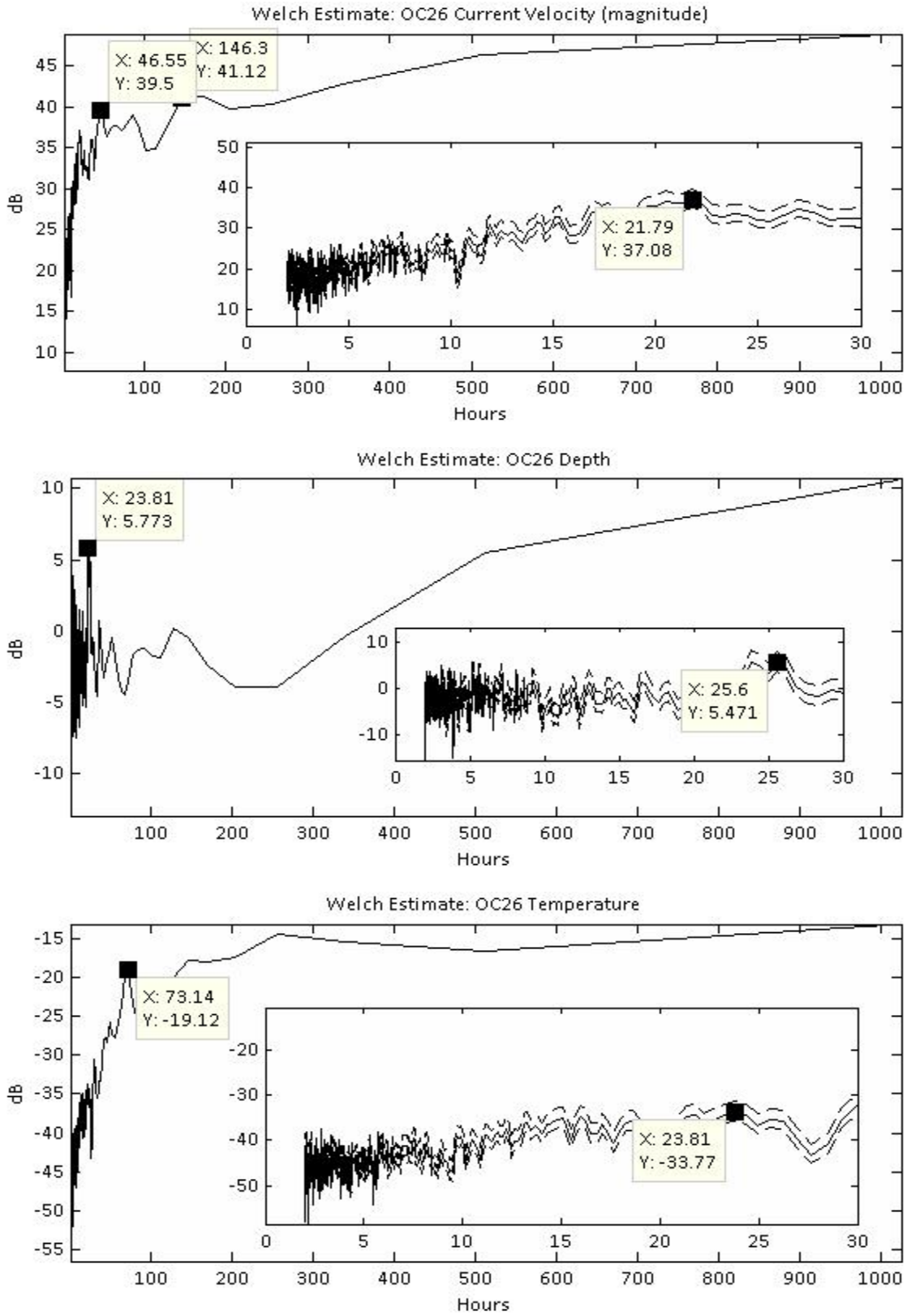

Figure 15. OC26 WOSA spectral estimations A) current velocity (magnitude) B) depth C) temperature The broken line in the inset represents a 95% confidence interval.

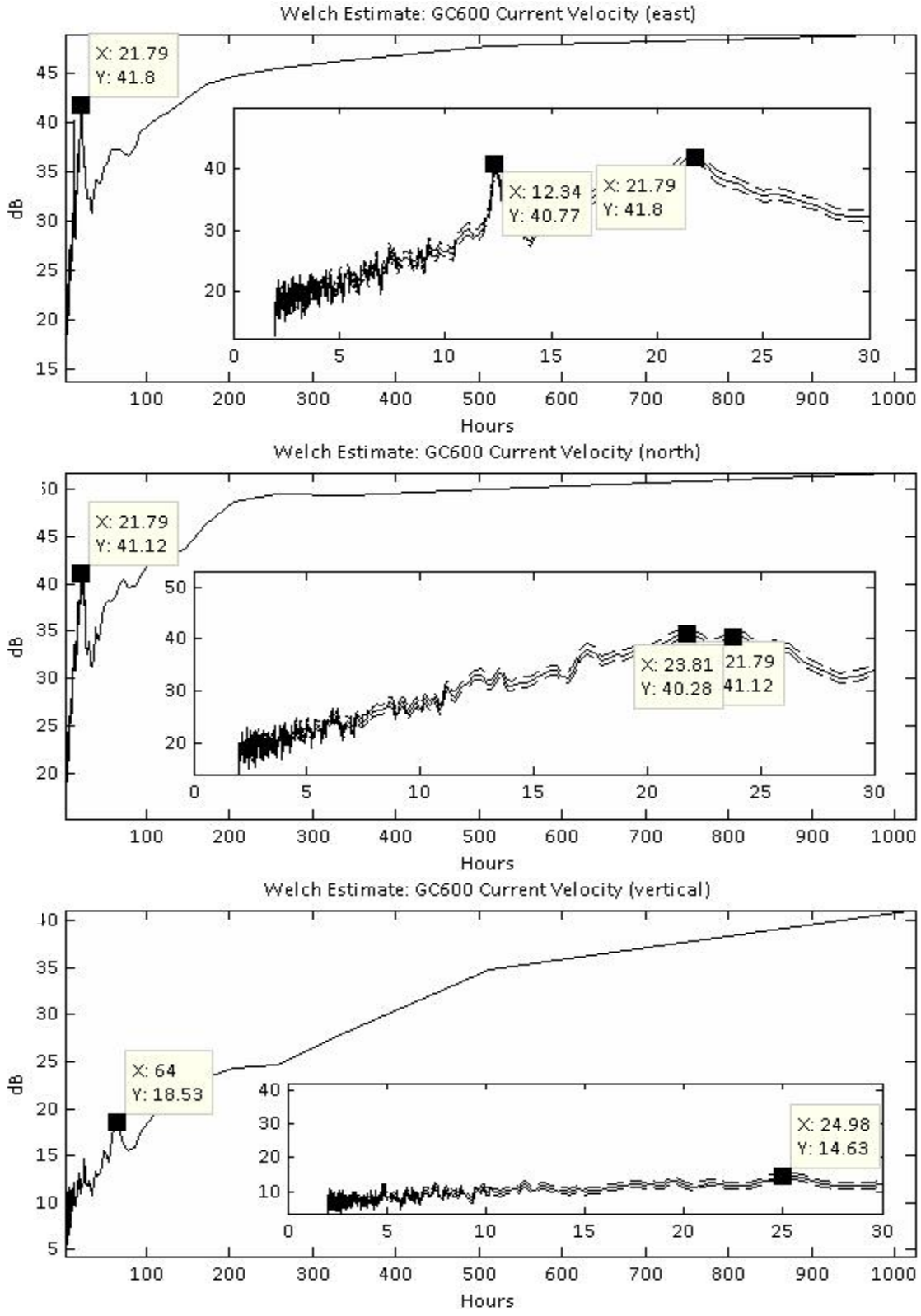

Figure 16. GC600 WOSA spectral estimations A) current velocity (east) B) current velocity (north) C) current velocity (vertical) The broken line in the inset represents a 95% confidence interval.

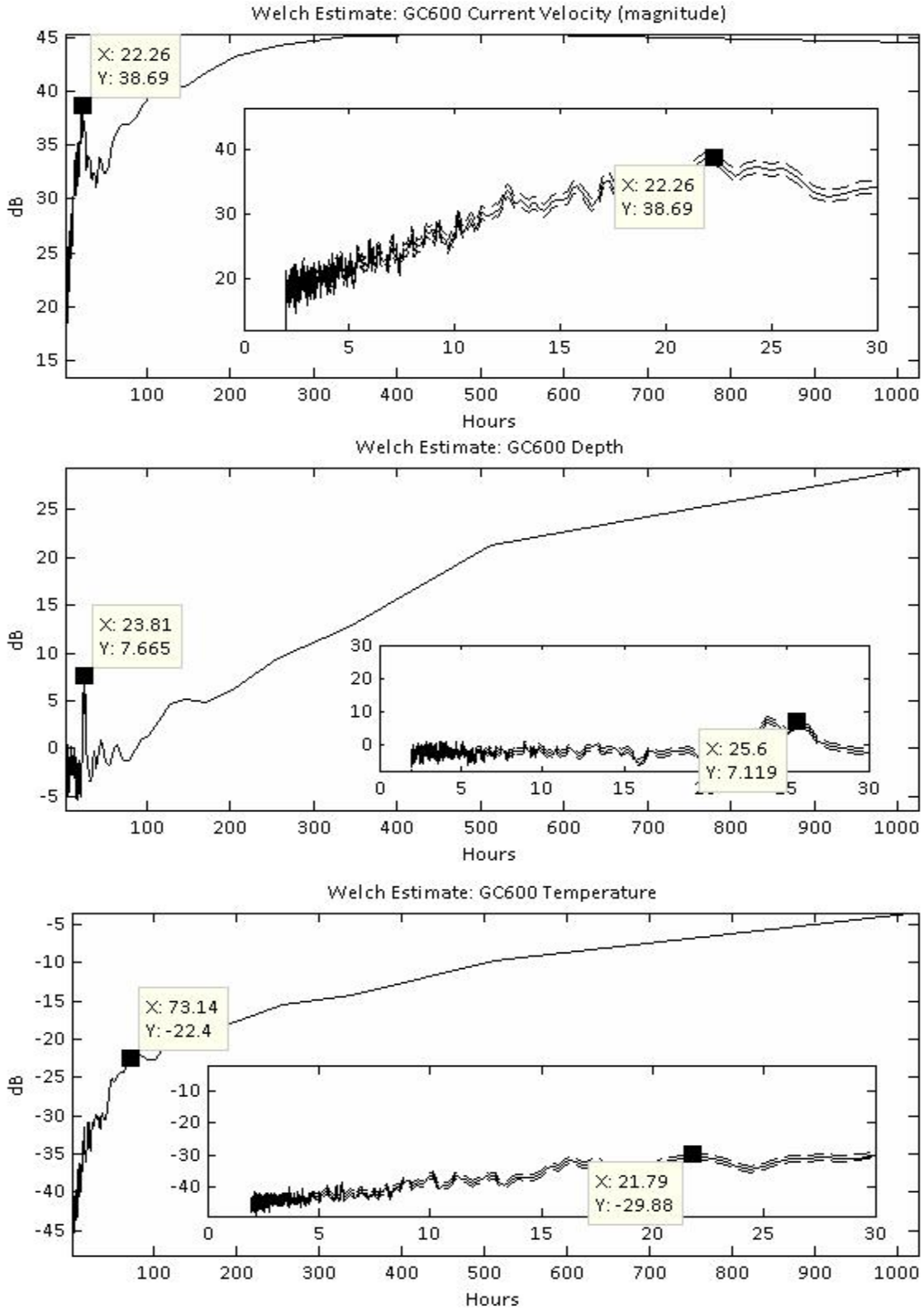

Figure 17. GC600 WOSA spectral estimations A) current velocity (magnitude) B) depth C) temperature The broken line in the inset represents a 95% confidence interval.

Bihourly Particle Counts

Averages. The average bihourly particle concentration for OC26 was ~4.5 particles per liter and the average bihourly particle concentration for GC600 was ~7.5 particles per liter. The night before September 2nd, particle concentrations were about twice the average for OC26, and beginning the morning of September 2nd, concentrations rose steadily, peaking late in the morning (Figure 18 and Figure 19). Concentrations remained well above average throughout the night of the 2nd and all day on the 3rd (Figure 19). The average particle concentration for September 2nd -3rd was ~22.8 particles per liter. Contemporary bihourly particle counts depict an average concentration of ~3.14 particles per liter at OC26 and an average concentration of ~7.40 particles per liter at GC600. The average bihourly aggregate volume per liter of seawater for the complete OC26 dataset was ~1.6 mm^3. On the morning of July 11, 2012 and the evening of October 19, 2012 about a sevenfold increase in aggregate volume was observed at OC26, as close to 35 mm^3 of aggregate volume per liter of seawater had entered the viewing chamber (Figure 20). The average aggregate volume per liter of seawater for September 2nd–3rd was ~6.5 mm^3 but close to 24 $mm^3 \cdot L^{-1}$ was found on the morning of September 2, 2012 (Figure 20). The average bihourly aggregate volume per liter of seawater for the complete GC600 dataset was ~2.2 mm^3 (Figure 21). Covering September 11, 2012 11:06 AM-December 28, 2012 2:14 PM, a contemporary average bihourly particle volume concentration graph depicts an average aggregate volume per liter of seawater of ~1.0 mm^3 at OC26 and an average aggregate volume per liter of seawater of ~2.2 mm^3 at GC600 (Figure 21).

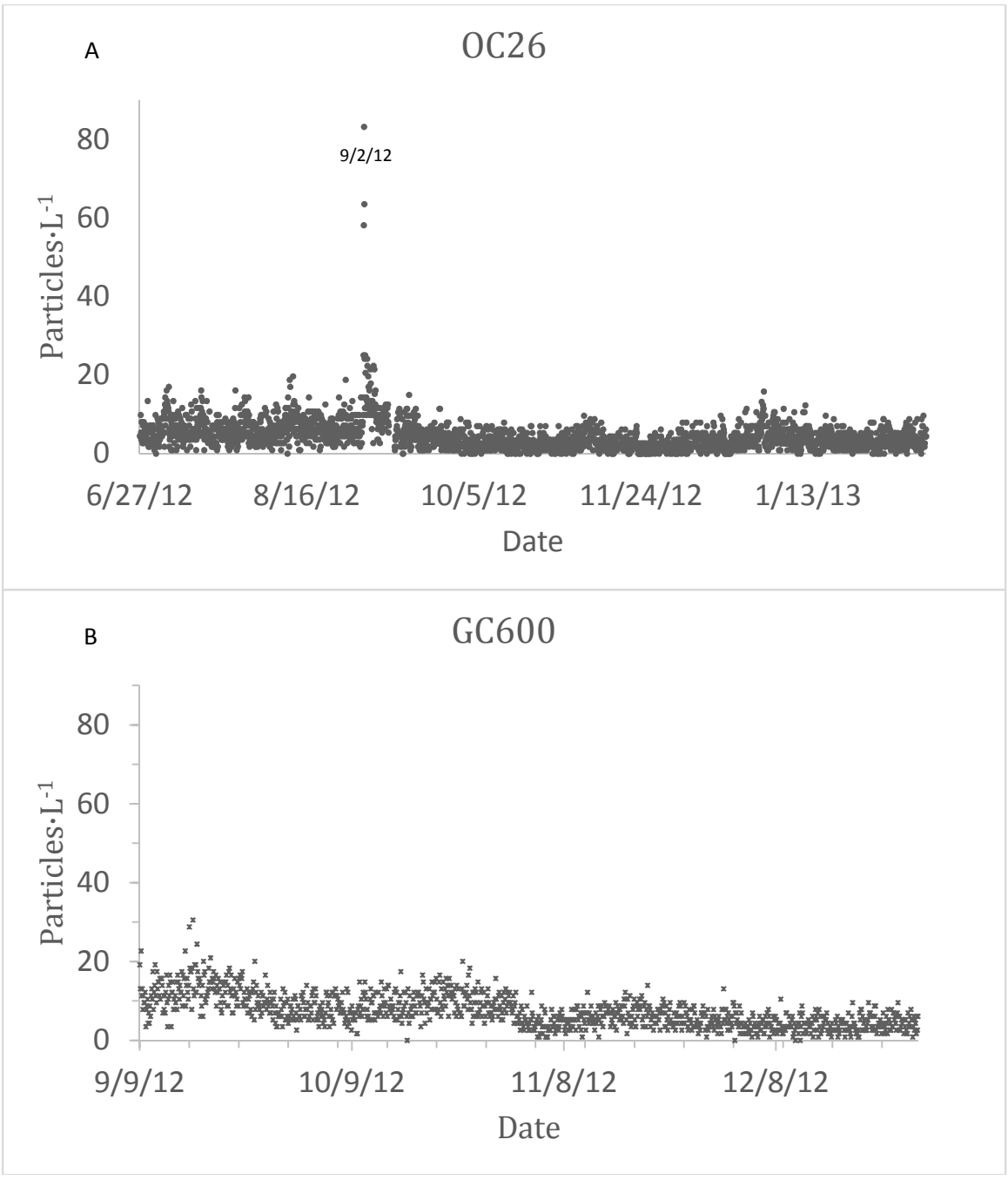

Figure 18. Particle concentrations A) OC26 B) GC600

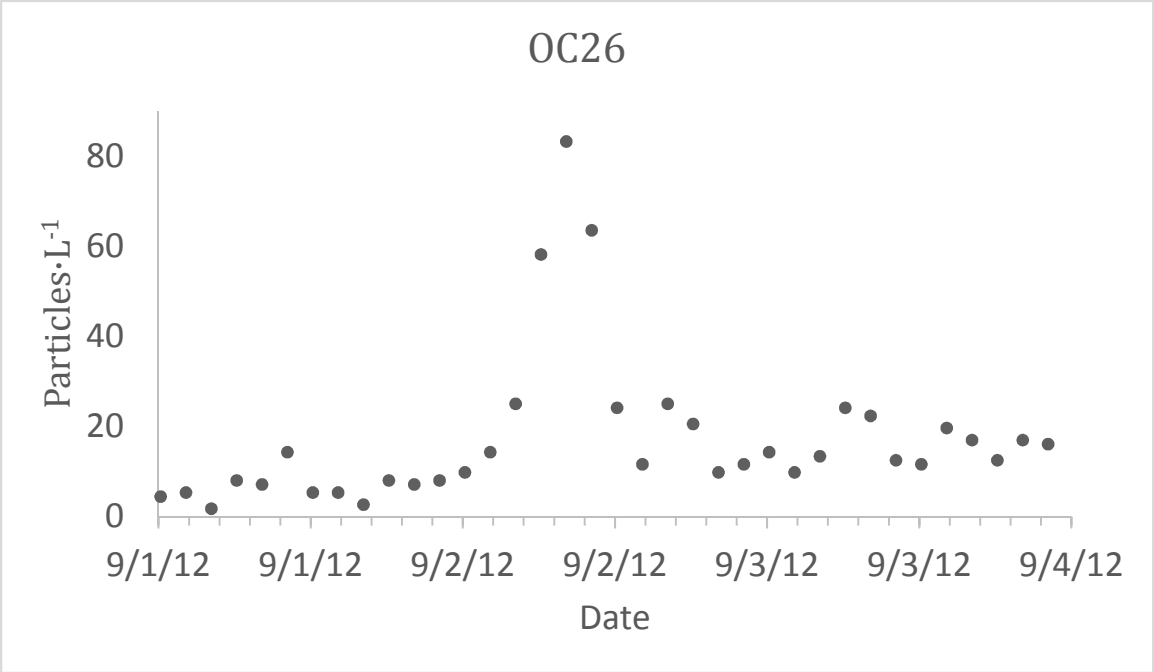

Figure 19. OC26 bihourly particle count (concentration) during Hurricane Isaac

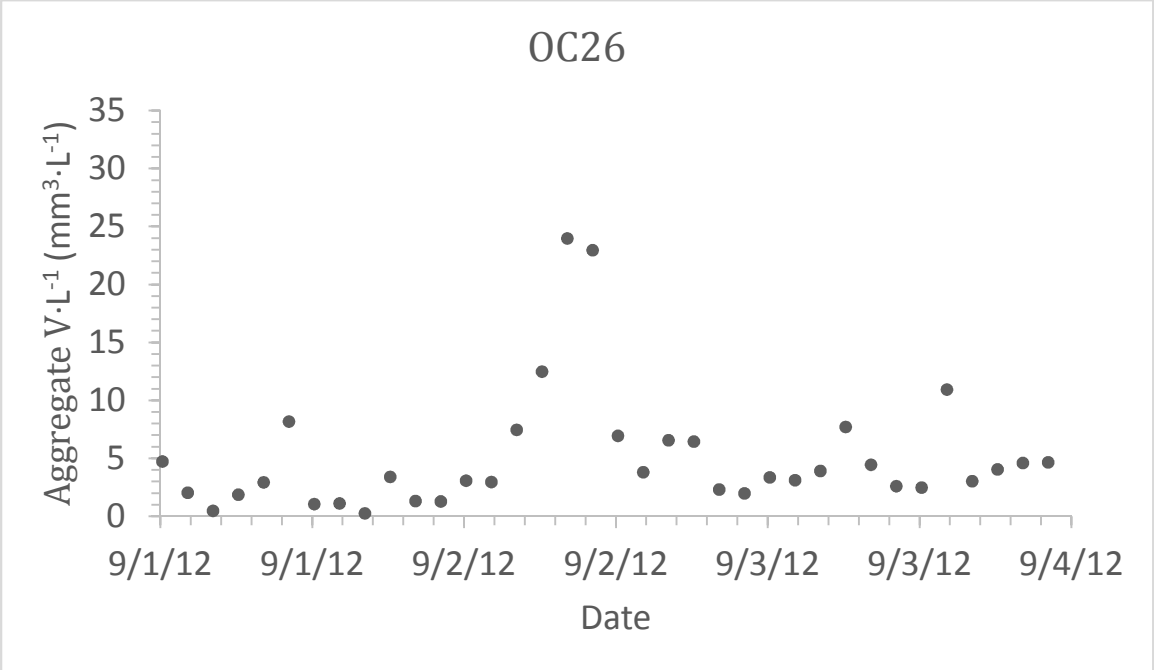

Figure 20. OC26 bihourly particle count (volume concentration) during Hurricane Isaac

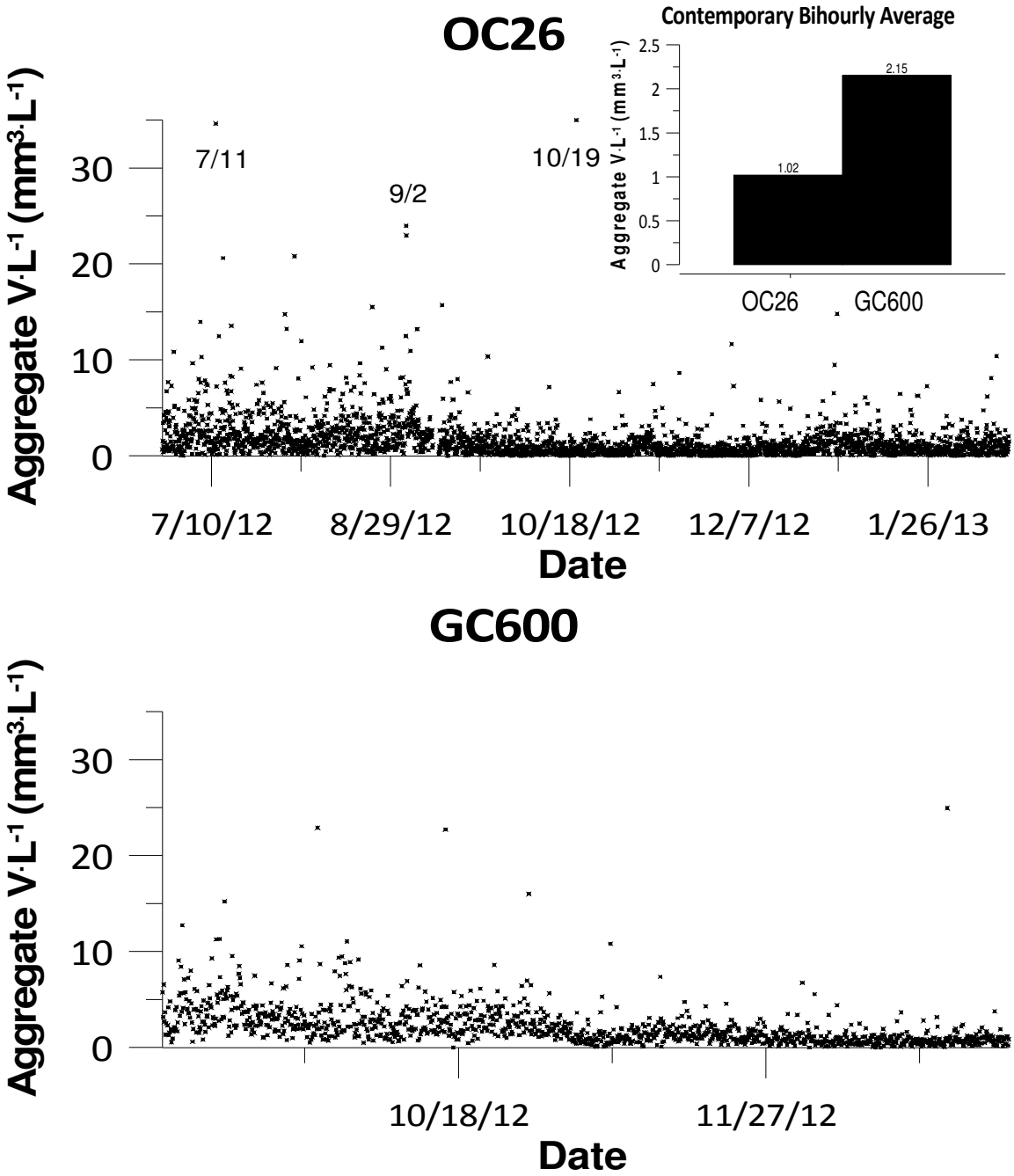

Figure 21. Bihourly aggregate volume concentrations vs time A) OC26 (contemporary averages inset) B) GC600

Periodicities. As an examination of periodicities of particle flux may provide insight into the particle source, WOSA from OC26 and GC600 bihourly counts are shown (Figure 22 and Figure 23). The data is from the particle counts and the aggregate volume concentrations. Hann windows of 720 hours and 90% overlap were used to

accentuate signals of less than a month in period. The broken lines on the plot insets outline the 95% confidence interval. At OC26 a peak is found at 29.68 hours in both the particle count and the particle volume concentration plots; however, the highest peaks found in the particle count WOSA are a biweekly peak at 341.3 hours and a weekly peak at 170.7 hours (Figure 22). A peak at 19.5 hours is found in both the particle count and the particle volume plots for GC600; however, the highest particle count peak was found at 227.6 hours (~9.5 days) and the highest particle volume concentration peak was found at 5.404 hours (Figure 23).

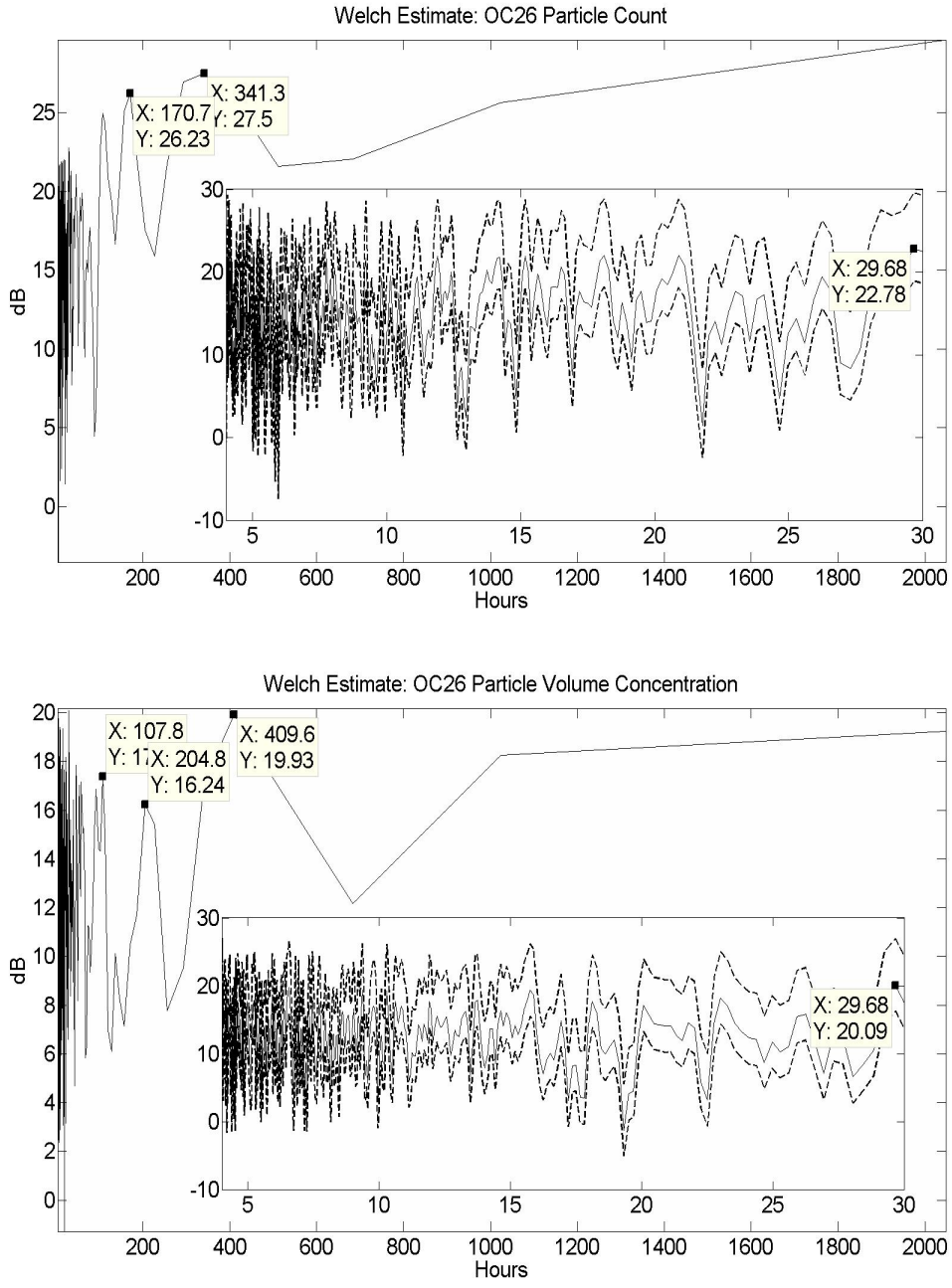

Figure 22. OC26 WOSA spectral estimations A) particle count B) particle volume concentration

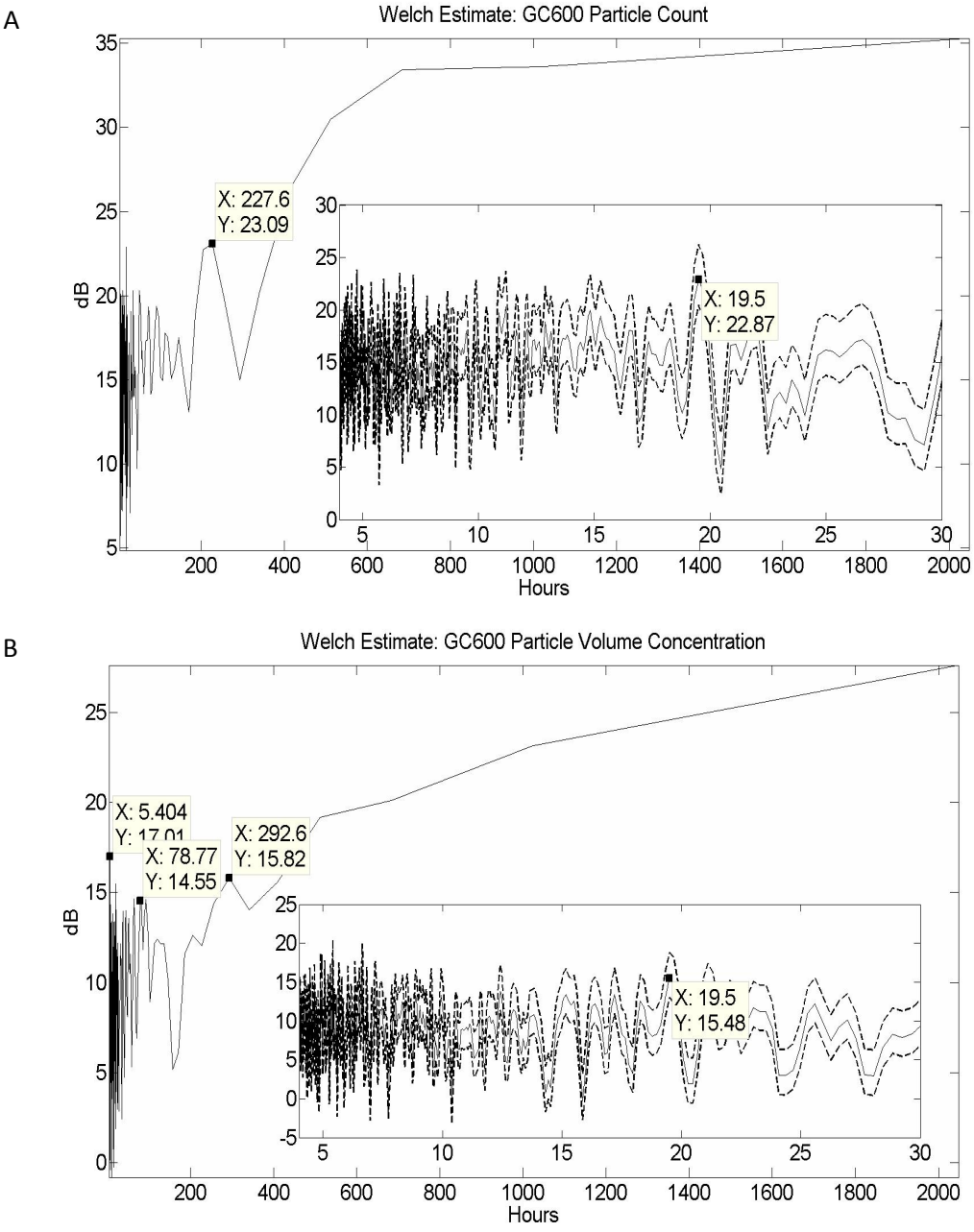

Figure 23. GC600 WOSA spectral estimations A) particle count B) particle volume concentration

Hurricane Isaac

"Snowstorm". Hurricane Isaac produced a "snowstorm" at OC26, depositing about a twentyfold increase of particles into the viewing chamber (Figure 18 and Figure 19). The end of August and early September storm event was associated with higher current velocities (Figure 11 and Figure 13) and greater particle numbers (Figure 18 and

Figure 19). Generally, during the tropical storm denser particles were associated with faster currents (Figure 24). An abrupt temperature drop of almost 0.1° C was recorded at OC26 that had started on August 30, coinciding with a decrease in current velocity (magnitude) that had approached 20.0 $cm \cdot s^{-1}$ (Figure 25). For two days the temperature remained just above 4.1° C, possibly indicating water from a different source had moved into OC26, associated with a northerly current direction that turned southerly on September 1st (Figure 25). The temperature increased on the morning of September 2, almost reaching 4.2° C, as a current turned towards the north (Figure 25 and Figure 26). Of velocity-assigned particles associated with the colder water on August 31 and September 1, the average settling velocity was 49.3 $m \cdot day^{-1}$ and the average diameter was 0.57 mm, resulting in an average density of 1.0326 $mg \cdot mm^3$ (by Equation 3), representing a 6% higher excess density than that of the September 2nd average and a 60% higher excess density than that of the OC26 dataset average. Across August 31th and September 1st, the average bihourly particle count was 6.8 particles and the average bihourly ESD was 0.93 mm. The average bihourly particle count and ESD for September 2 were 33.3 particles and 0.80 mm, respectively. For the entire OC26 data set, the averages were 5.1 particles and 0.80mm. An almost 0.1° C rise in temperature was observed on the morning of September 2nd that preceded a current direction shift to the south as the temperature decreased (Figure 26). The average density of particles assigned a settling velocity from the morning to about noon of September 2 was 1.0326 $mg \cdot mm^3$ (by Equation 3). The average density of particles observed on this morning was the same as those associated with the cold water. That morning, the north current strengthened, deposition abated, and the particulate load increased as evidenced by the increased ADCP range (Figure 13, Figure 25, and Figure 26). This north current accelerated to about 15

$cm \cdot s^{-1}$ before decreasing in velocity (magnitude), at which point particle deposition intensified (Figure 25 and Figure 26).

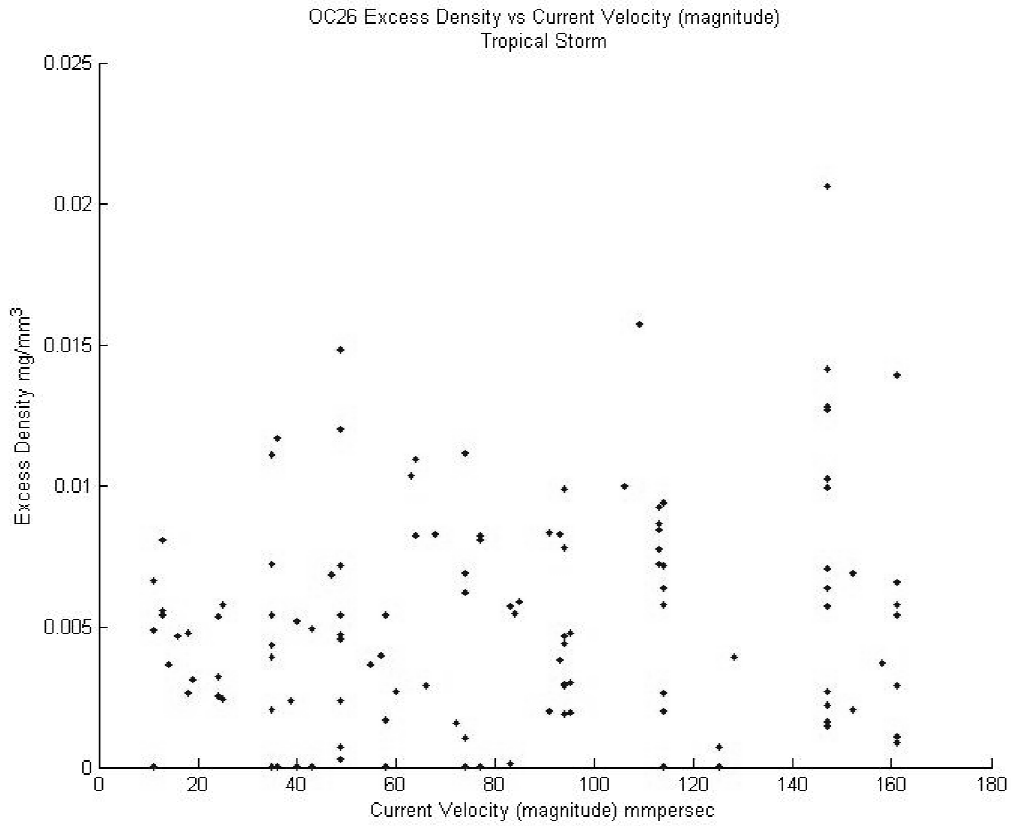

Figure 24. OC26 particle excess density vs current velocity (magnitude) during Hurricane Isaac

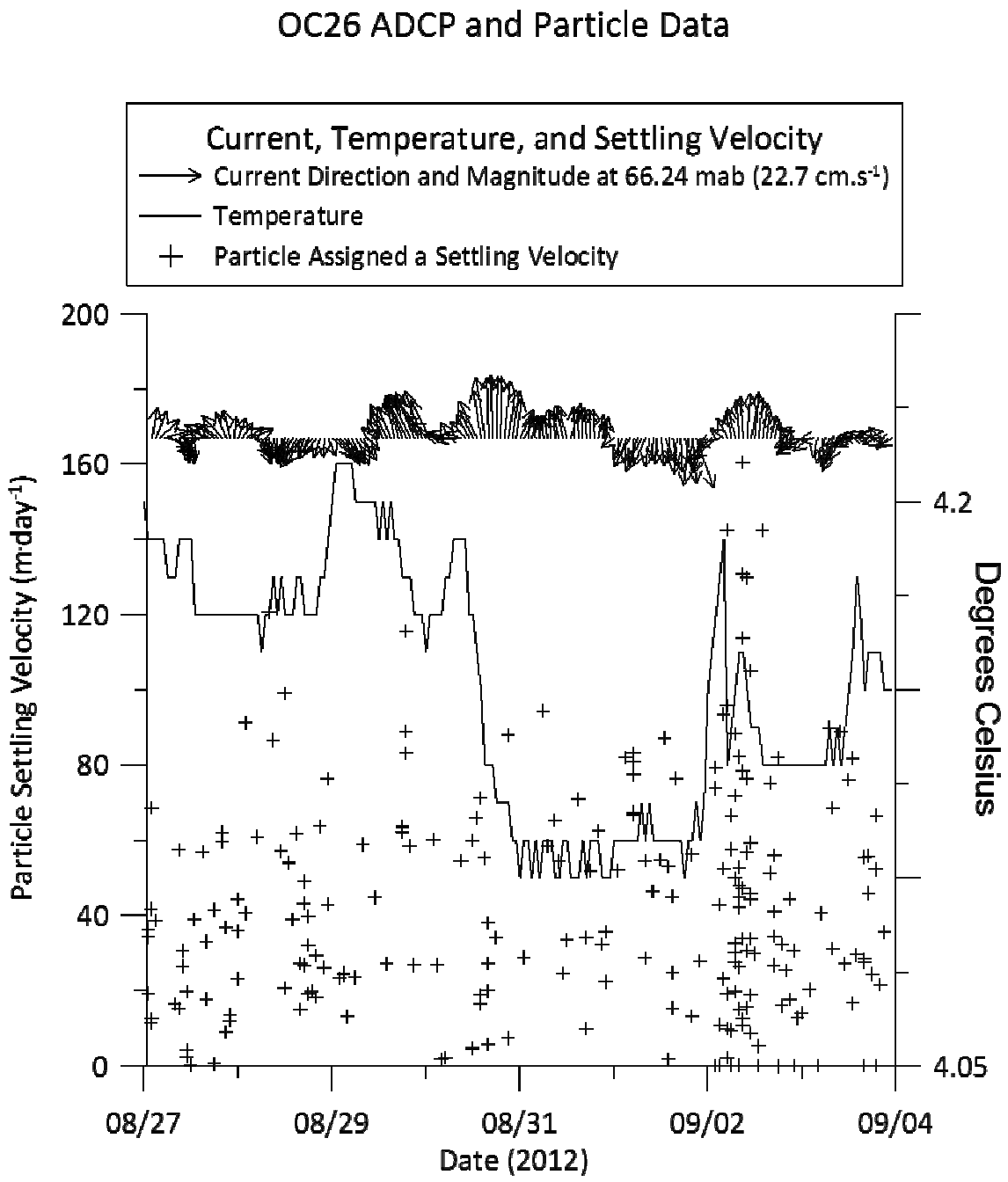

Figure 25. OC26 ADCP and particle data: current velocities (magnitude) and directions to are from 15-21.23 mab

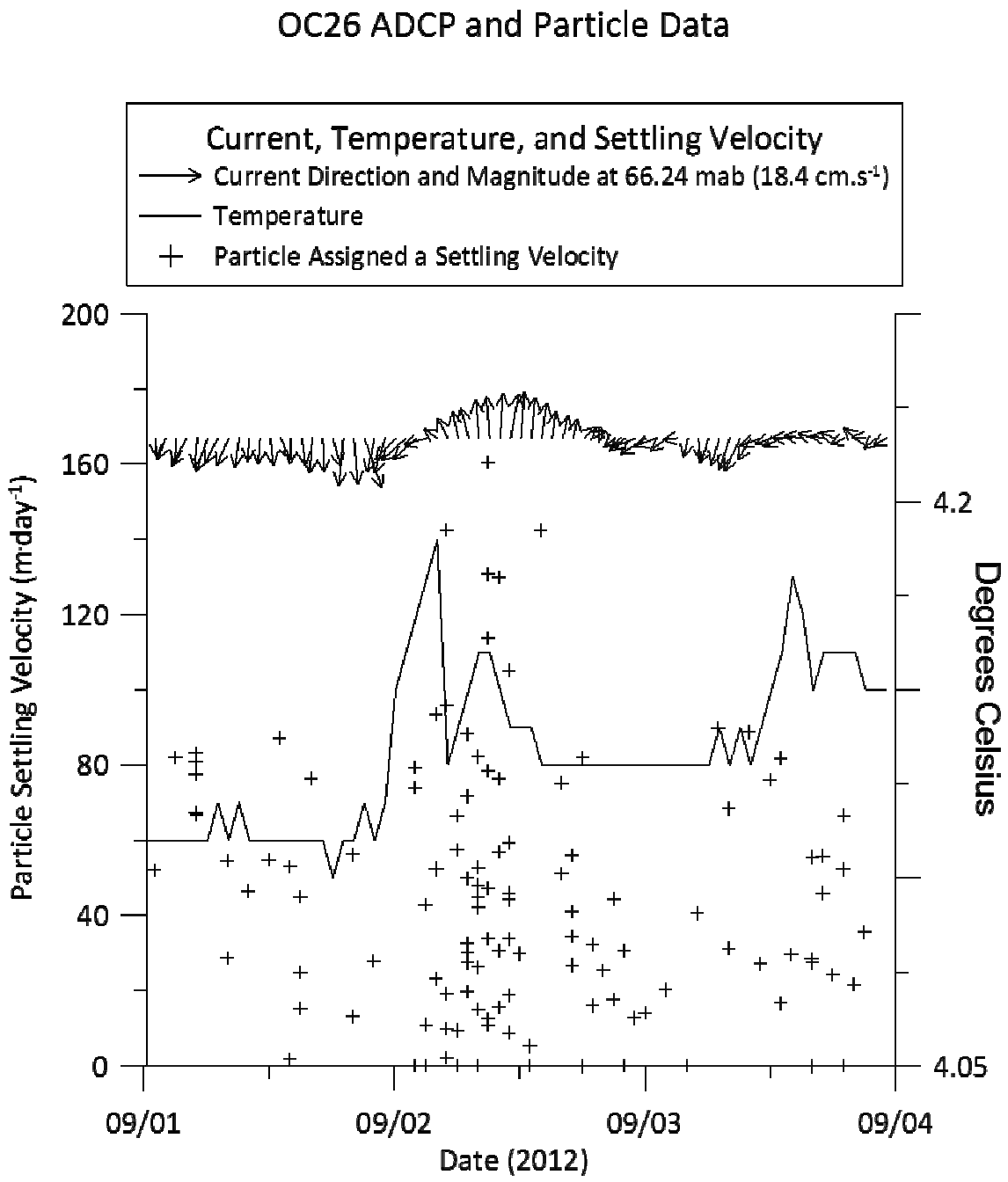

Figure 26. OC26 ADCP and particle data: current velocities (magnitude) and directions to are from 15-21.23 mab

High current velocity and high deposition rate. At GC600, the largest particle flux immediately following the September deployment may have occurred due to a fast current September 15th-16th associated with a change in water type as 4.3° C water left

the site on September 14th (Figure 27). On the evening of September 15th, particle flux seemingly increased with a northeasterly current, and current velocity reached about 15 $cm \cdot s^{-1}$ to the north on the morning of the 16th when flux was still high (Figure 27). This northerly current was associated with the largest particle concentration observed at GC600 as over 30 particles per liter were imaged on September 16th (Figure 18 and Figure 27). The average particle concentration the first GC600 deployment was 4.5 particles per liter.

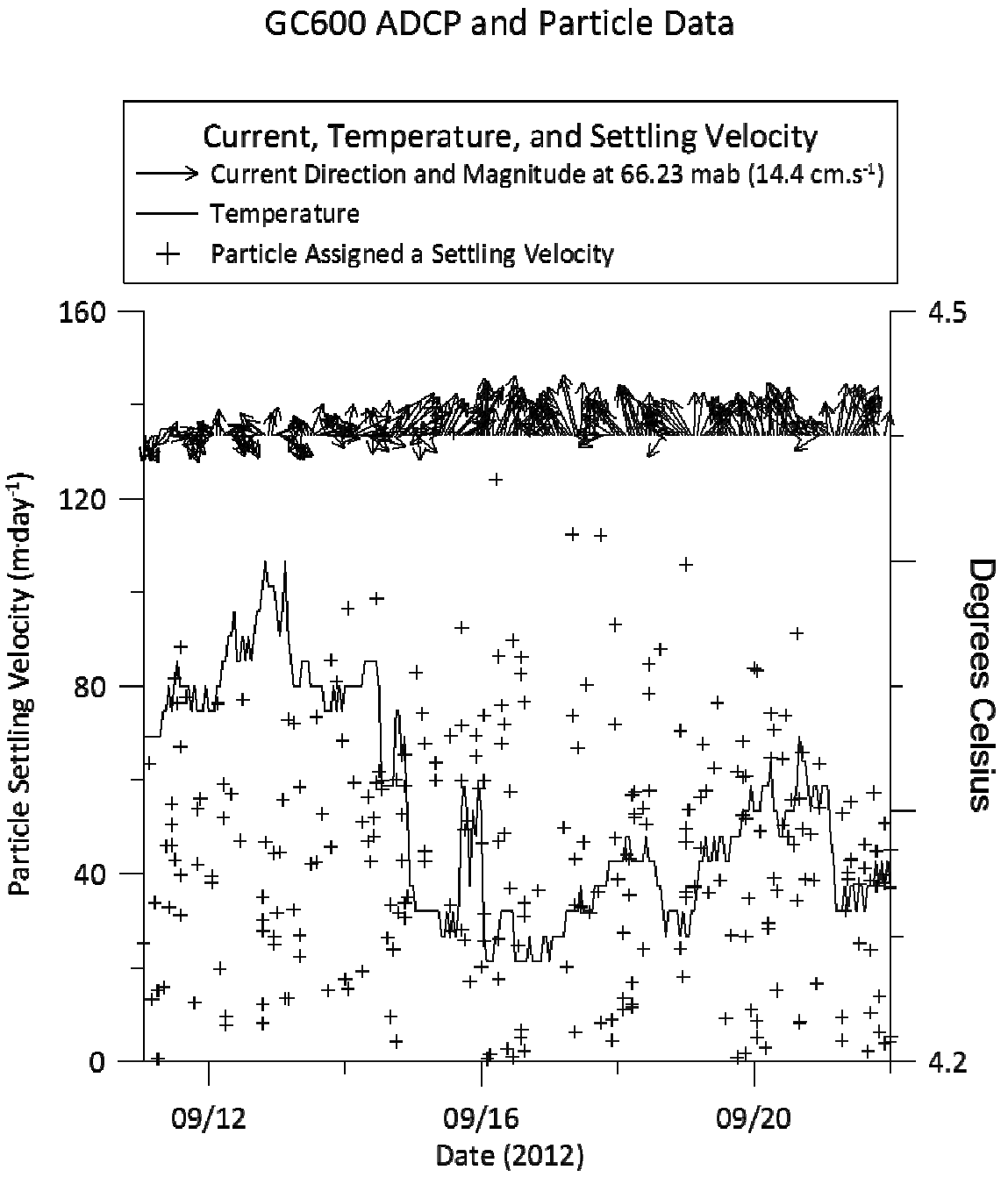

Figure 27. GC600 ADCP and particle data: current velocities (magnitude) and directions are from 15-21.23 mab

Marine Snow Profiles

OC26 Profiles

Bottom layer of suspended particles. An increase in beam attenuation was seen at 250 mab indicating the presence of a thick bottom layer of suspended particles. All profiles had a distinct turbidity front in the uppermost part of this layer. The fronts were characterized by a sharp transition between this layer and the overlying water column.

In situ aggregate numbers and sizes. The MSC casts showed a mostly uniform distribution of total aggregate abundance in the uppermost 1200 m of the water column (~20 aggregates·L^{-1}) (Figure 28, Figure 29, and Figure 30). Aggregate abundance sharply increased in the bottom layer of suspended particles, reaching levels within the turbidity front of ~130 aggregates·L^{-1} (Figure 28). Most of the aggregates were in the smaller size range (0.5-1 mm in diameter); however in cast #3, macro aggregates >1 mm in diameter increased in relative abundance below the turbidity front, constituting 40% to 50% of the total numbers of aggregates near the seafloor (Figure 28, Figure 29, and Figure 30).

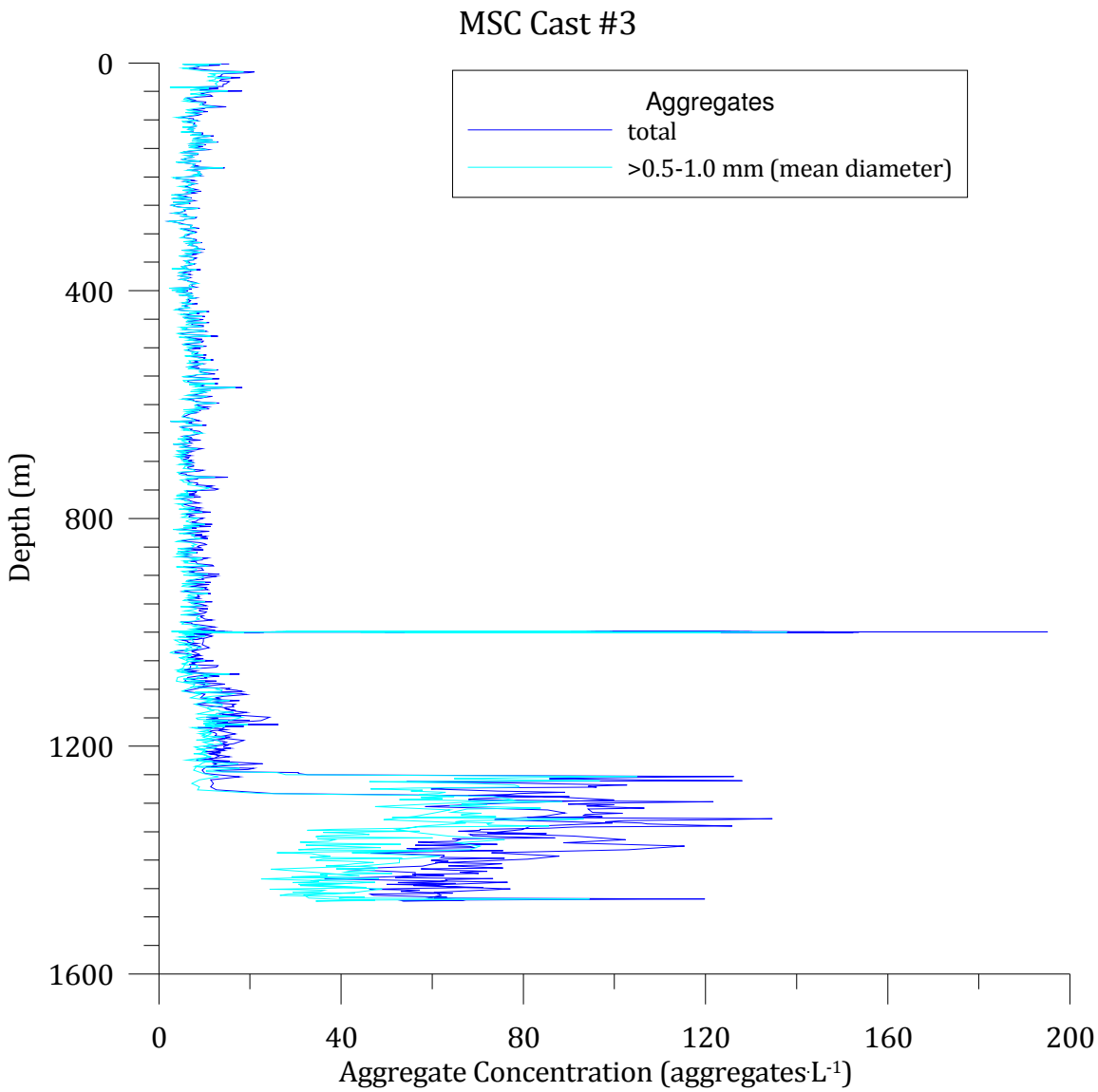

Figure 28. Marine snow profile from Cast #3 near OC26 showing small and total aggregate concentrations

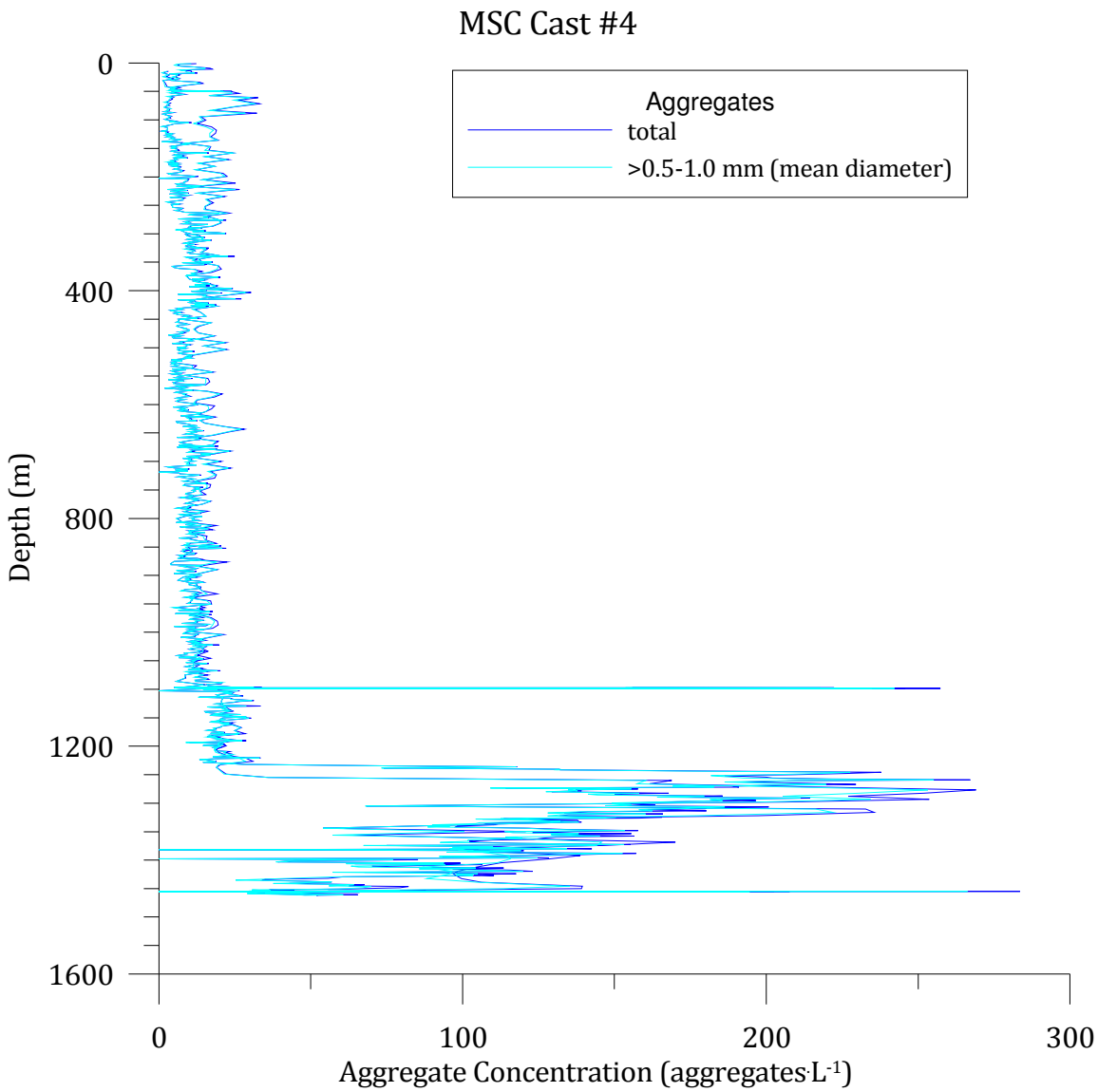

Figure 29. Marine snow profile from Cast #4 near OC26 showing small and total aggregate concentrations

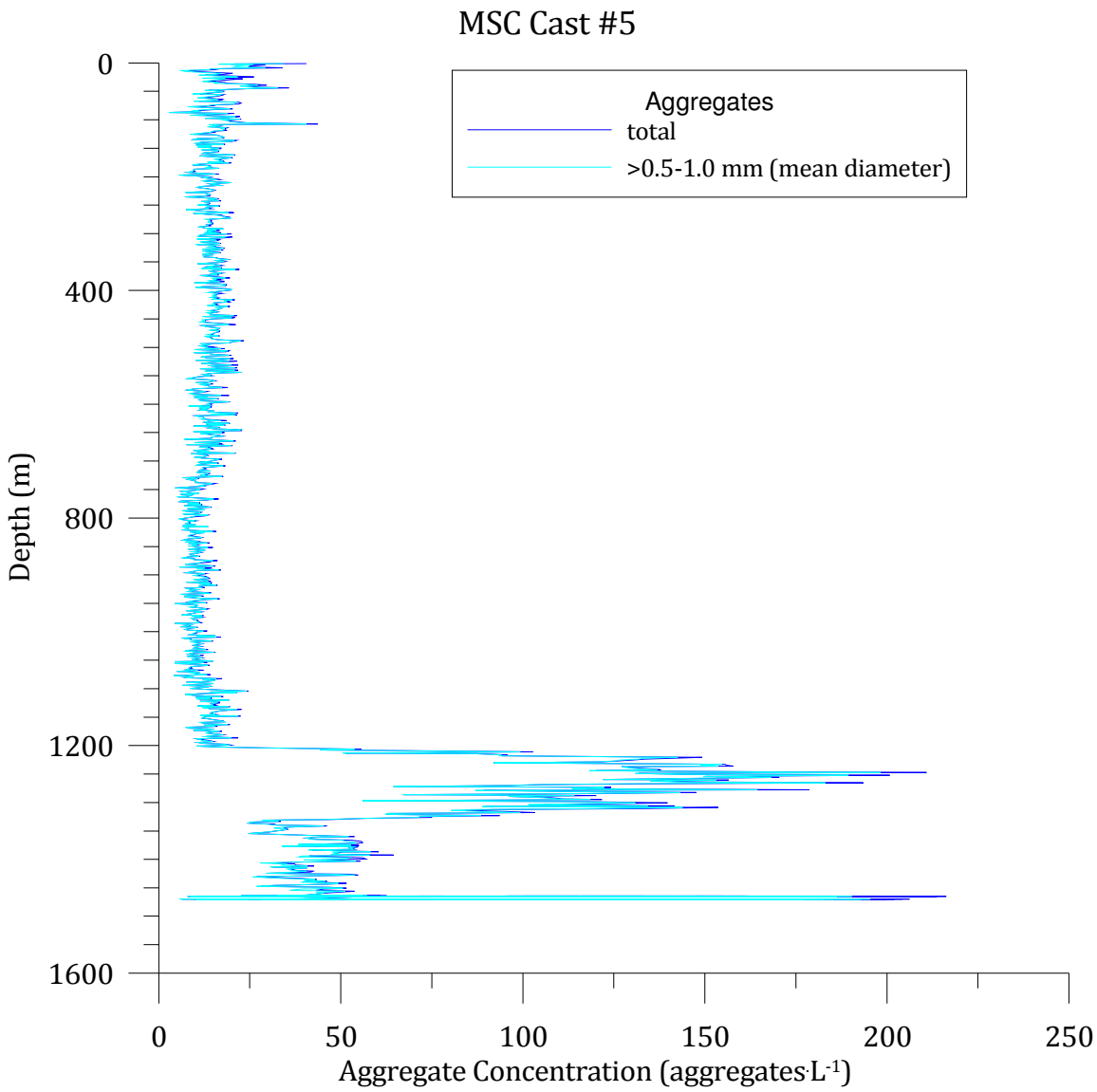

Figure 30. Marine snow profile from Cast #5 near OC26 showing small and total aggregate concentrations

Sediment Trap Data

OC26 Sediment Trap Data

Top vs bottom trap. Material collected in the OC26 sediment traps from June 28, 2012 to September 8, 2012 was analyzed for dry weight (DW), particulate inorganic matter (PIM), particulate organic matter (POM), particulate inorganic carbon (PIC), particulate organic carbon (POC), and particulate organic nitrogen (PON) by (Figure 32)

(Passow U. , 2014). The analyses were performed on material collected over 18 day intervals. Particulate carbon (PIC+POC) quantities for both sediment traps at OC26 are also graphed (Figure 32).

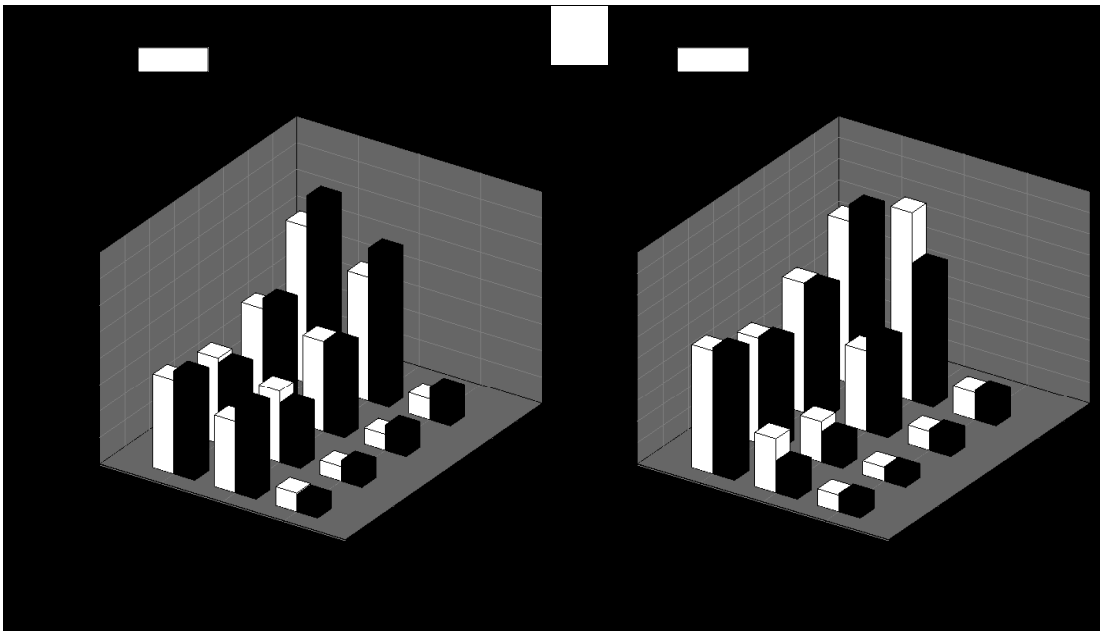

Figure 31. OC26 sediment trap data A) DW, PIM, and POM B) POC, PIC, and PON (Passow U. , Personal Communication, 2014)

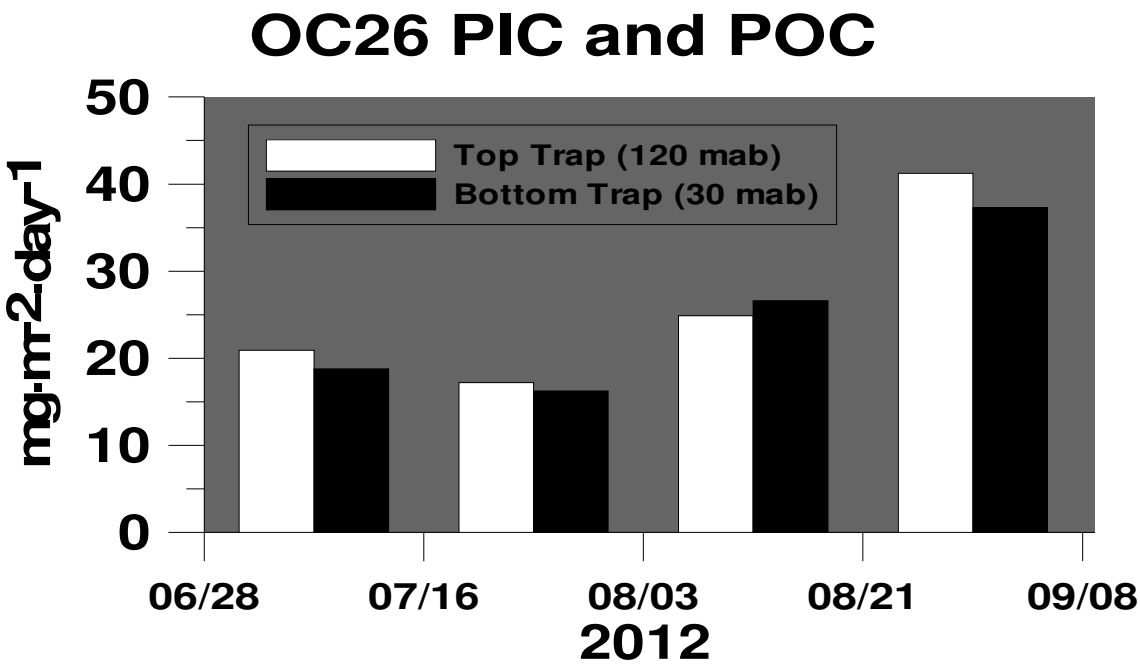

Figure 32. OC26 PIC and POC (Passow U. , Personal Communication, 2014)

GC600 Sediment Trap Data

Dry weight. Material collected in the GC600 sediment trap from September 10, 2012 12:00 PM to April 25, 2013 11:54 AM was analyzed for dry weight. The analysis was performed on material collected over 17.85 intervals (Figure 33).

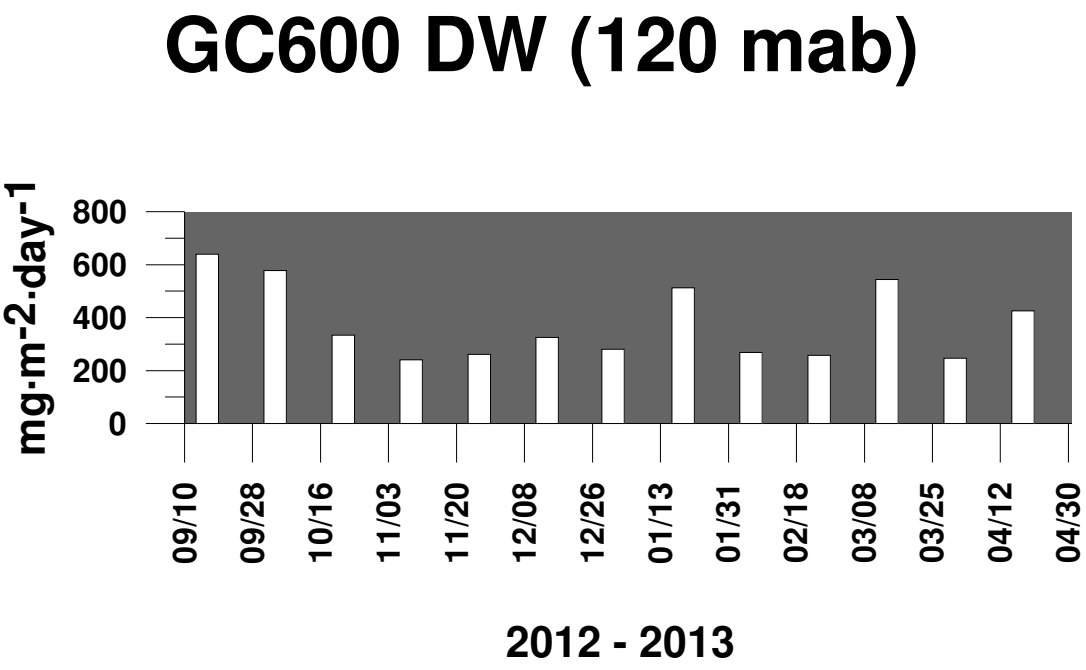

Figure 33. GC600 dry weight (Passow U. , Personal Communication, 2014)

CHAPTER IV

DISCUSSION

Settling Velocity

Ecological Implications

Oil reached the seafloor. Knowing where 1.078 millions of barrels of oil ended up would allow study of ecosystem effects of that oil. Due to studies such as that of White et al., 2014, it has been established that oil did make it to the seafloor in areas underneath the oiling footprint. Core samples showed oil deposition on the seafloor between May and September of 2010, and a dirty blizzard layer was found in November (Joye et al., 2014). If the missing oil had contributed to the surface slick it could have been redistributed by marine snow falling below the mixed layer. The formation of large oiled aggregates that disappeared in a matter of weeks may have transported a significant portion of the oil to the sediments beneath the surface slick or to as of yet unknown locations. Passow et al.'s (2012) determination of spill associated aggregate settling velocities to be 68-553 $m \cdot day^{-1}$ along with the results of averaging OC26 current velocities (1.13 $cm \cdot s^{-1}$ having a northerly direction) allow for a sedimentation range of ~3-23 km to the north in 1600 m of water (Figure 11).

Processes disallowing burial. Before an aggregate can get buried in the sediment; there are several processes that may affect it and any oil it may contain. Considering the depth and average settling velocities of the two study sites, a transit through the entire water column would have taken ~51 days at OC26 and ~33 days at GC600. Throughout its fall, it can collide with and aggregate with other particles, creating a larger particle that has a faster settling velocity. The particle can disaggregate as well, decreasing the settling velocity. Microbes associated with a surface particle may be transported to depth

as the particle settles. Constituents are available to bacteria that are passengers of the aggregate, or the particle may be consumed entirely by a deep water denizen. Once on the seafloor, a particle may be suspended by strong currents such as those exceeding 12.5 $cm \cdot s^{-1}$ at OC26 (Figure 11). When a particle is brought back into the water column from the seafloor it may again be subject to biological degradation and ingestion. It may also be relocated to another community before it finally gets buried in seafloor sediment. Considering the average current velocity (magnitude) at both sites, a suspended particle that took one day to settle back to the seafloor would have travelled laterally ~363 m at OC26 and ~441 m at GC600.

Site Comparison of Settling Velocity

First hypothesis. Particles at OC26 were not found to have faster settling velocities than particles at GC600. Of the particles from OC26 assigned a settling velocity, the average velocity was 32.4±22.7 $m \cdot day^{-1}$ and the average diameter (mean) was 0.59±0.09 mm. For GC600, these averages were 42.3±24.3 $m \cdot day^{-1}$ and 0.61±0.10 mm. The average contemporaneous settling velocity and diameter (mean) at OC26 was 30±20 $m \cdot day^{-1}$ and 0.59±0.09 mm, and the average contemporaneous settling velocity and diameter (mean) at GC600 was 40±20 $m \cdot day^{-1}$ and 0.6±0.1 mm (Table 4). As calculated using settling velocities, the average OC26 density and ESD were 1.031±0.002 $mg \cdot mm^{-3}$ and 0.61±0.09 mm, and the average GC600 density and ESD were 1.031±0.002 $mg \cdot mm^{-3}$ and 0.6±0.1 mm. Thus, the hypothesis that OC26 would have particles with higher settling velocities due to increased densities was unsupported.

Particle Source

Time Series

Second hypothesis. No associations between particle suspension and currents were made as a result of the WOSA. The Welch estimate for the OC26 particle count failed to produce a distinct signal within a 30 hour period. There are peaks at 170.7 and 341.3 hours, or 7.11 and 14.22 days (Figure 22). These peaks are not seen on the GC600 Welch estimate for the particle count; instead, a signal of 19.5 hours and 227.6 hours (9.48 days) were observed (Figure 23). A 29.68 hour peak is found in both the particle volume concentration estimate as well as the particle concentration estimate for OC26, and there is a 107.8 hour (4.9 days) signal for particle volume concentration that is found for particle concentration there as well (Figure 22). These peaks may be seen in the current velocity WOSA; however, these periods were not prominent (Figure 14 and Figure 15). The peak with the highest magnitude in the OC26 particle volume concentration estimate is at 409.6 hours (17.1 days) (Figure 22). At GC600, the highest particle volume concentration peak is found at 5.404 hours, possibly a result of primary flux cycles (Figure 23). A peak of 19.5 hours is found in the particle volume concentration as well as in the particle concentration estimate for GC600 (Figure 23). No correlation was made between current and deposition periodicities, thus the second hypothesis was supported.

Sediment traps flux information. The sediment traps provided flux information (Figure 31, Figure 32, and Figure 33). At OC26, the bottom trap mirrored the top trap, and for every interval except for July 16-August 3, a period of relatively weak currents (Figure 11), there was greater flux recorded by the bottom trap, indicating local suspension (Figure 31). There was more PIM, POC, and PIC collected in the upper trap

than the lower trap during the period of July 16-August 3 (Figure 31). PIC was more abundant in the upper trap during the August 21st-September 9th interval as well (Figure 31). More POM was found in the bottom trap for every interval except the first (Figure 31). As current speeds were observed to have been relatively low during this period, local suspension may have abated (Figure 11). Only during the collection period encompassing the tropical storm, August 21-September 8, and only in the uppermost trap, did the level of PIC (22.2 $mg \cdot m^2 \cdot day^{-1}$) exceed the level of POC (19 $mg \cdot m^2 \cdot day^{-1}$) (Figure 31). More PON found in the lower trap in all intervals supports rebound flux, local suspension of particles not chemically degraded (Figure 31). The average POC/ PON ratio in the top trap was 6.9 and the average in the bottom trap was 6.6, indicating old material suspended from the seafloor may not have produced a signal in the bottom trap. At GC600, there was a general decrease in dry weight flux after the summer ended until mid-January, possibly reflecting a decline in primary flux (Figure 33).

Chlorophyll a. Surface chlorophyll a levels during the intervals of the OC26 sediment trap remained about 0.3 $mg \cdot m^3$ above OC26 throughout the deployment. Chlorophyll a was about 0.4 $mg \cdot m^3$ from June 17th through July 27th, a period nearly encompassing the first two sediment trap intervals (Figure 31, Figure 34, and Figure 35). The chlorophyll a concentration at OC26 was 0.2 $mg \cdot m^3$ July 27th through September 5th, a period that nearly corresponds to the last two sediment trap intervals in which an increase in sedimentation was observed (Figure 31, Figure 36, and Figure 37). Considering primary flux settling velocities to be 100s $m \cdot day^{-1}$ (Passow et al., 2012), a signal caused by a bloom would probably be received by the OC26 sediment traps, which were about 1400 m deep, within 2 weeks of any bloom. As no blooms were apparent at OC26 in the month and half preceding the increase in material seen in the third sediment

trap interval and 2 months preceding the even greater increase in material in the fourth interval, primary production at OC26 was not likely responsible for the increased sedimentation seen from June 30th through September 8th.

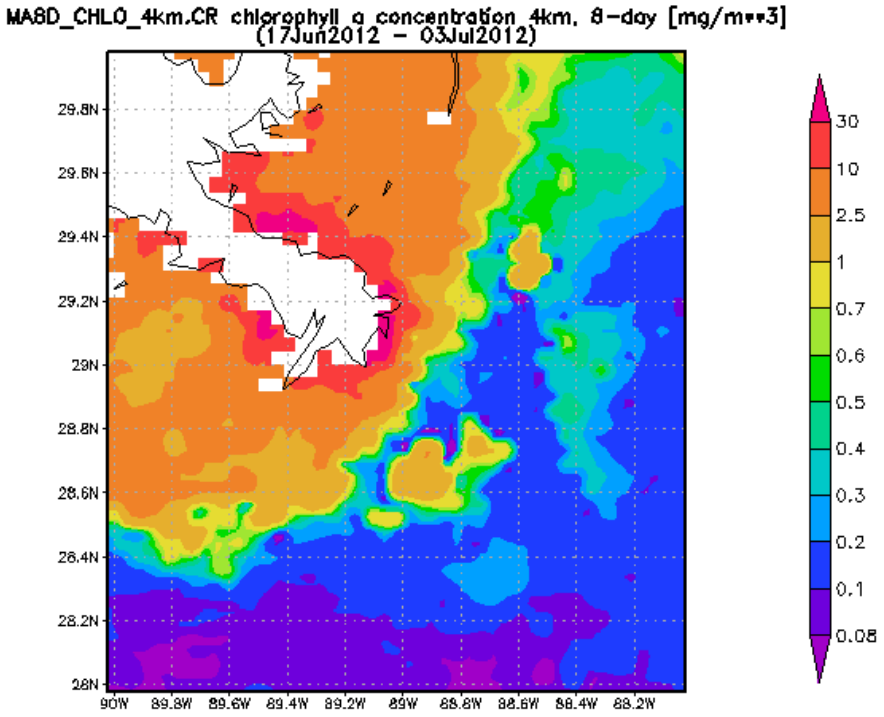

Figure 34. OC26 surface chlorophyll a concentration (17Jun2012 - 03Jul2012) Analyses and visualizations used in this paper were produced with the Giovanni online data system, developed and maintained by the NASA GES DISC (Acker & Leptoukh, 2007).

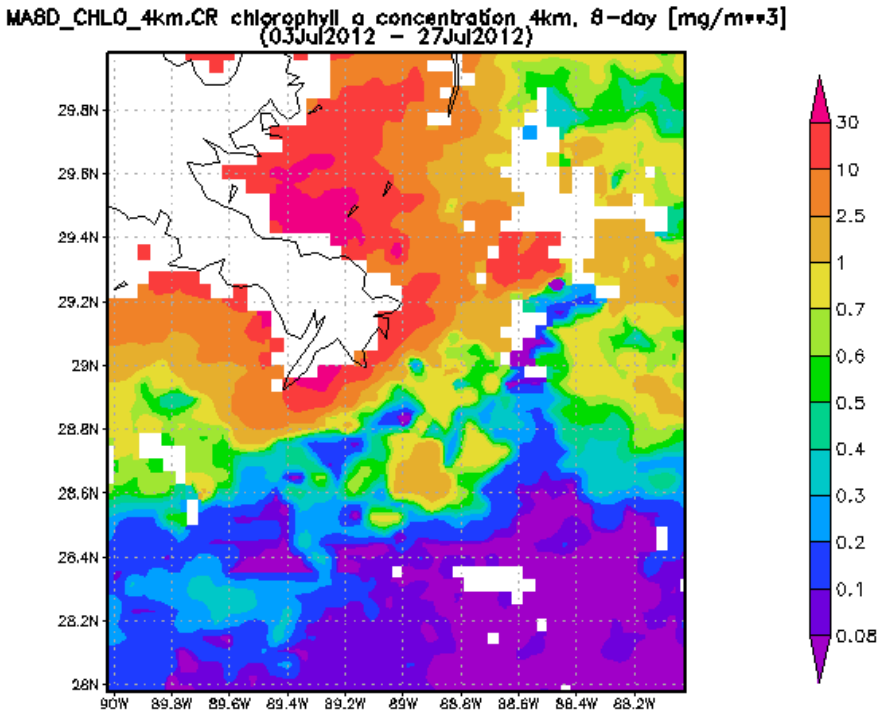

Figure 35. OC26 surface chlorophyll a concentration (03Jul2012 - 27Jul2012) Analyses and visualizations used in this paper were produced with the Giovanni online data system, developed and maintained by the NASA GES DISC (Acker & Leptoukh, 2007).

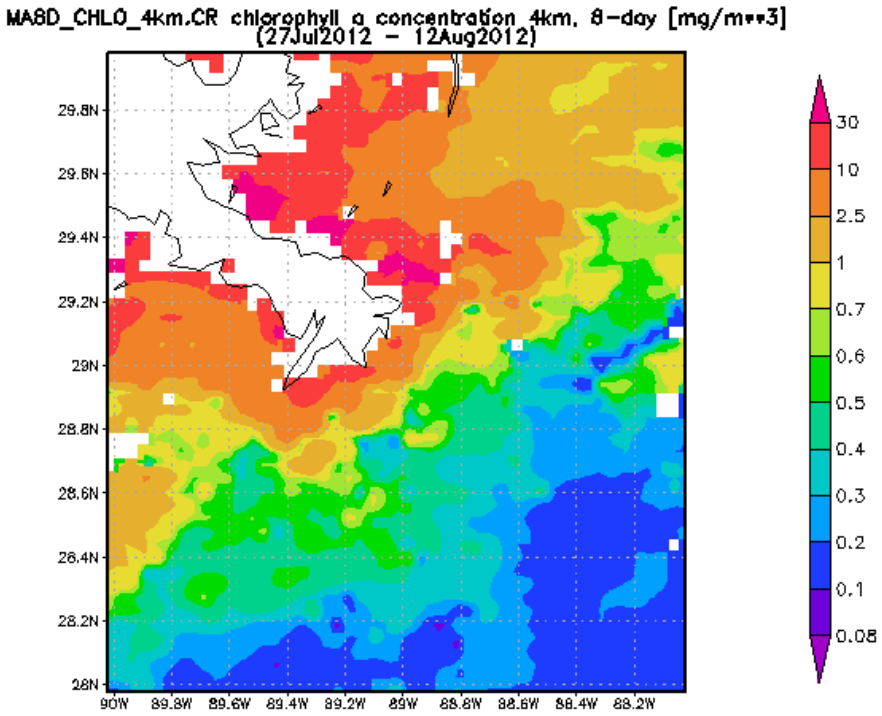

Figure 36. OC26 surface chlorophyll a concentration (27Jul2012 - 12Aug2012) Analyses and visualizations used in this paper were produced with the Giovanni online data system, developed and maintained by the NASA GES DISC (Acker & Leptoukh, 2007).

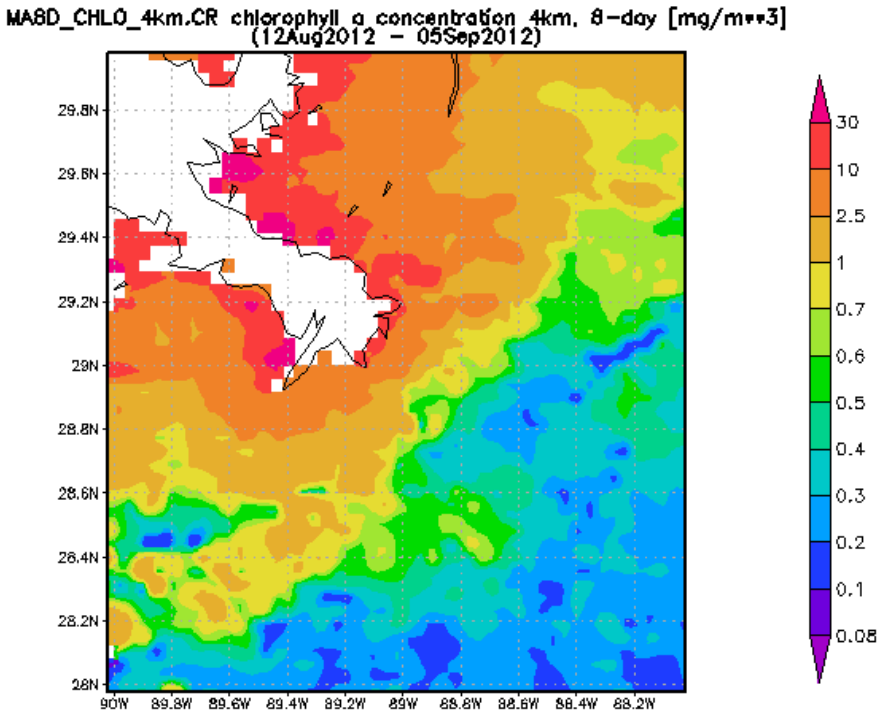

Figure 37. OC26 surface chlorophyll a concentration (12Aug2012 - 05Sep2012) Analyses and visualizations used in this paper were produced with the Giovanni online data system, developed and maintained by the NASA GES DISC (Acker & Leptoukh, 2007).

Marine Snow Profile

Suspended layer near the bottom. A thick bottom suspended layer was detected in the deep Mississippi Canyon (Station OC26) over an area of at least 3.5 km^2. This layer may have formed as a result of transport of shelf sediments down the Mississippi Canyon. A relationship between Hurricane Isaac and the presence of the layer deep in the Mississippi Canyon two weeks after the hurricane made landfall is plausible. Peak velocities of down-canyon turbidity currents during the investigation period likely exceeded 8 cm s^{-1}, based on previous observations. The first Marine Snow Camera cast (cast #3; Figure 8) also showed elevated numbers of macro aggregates near the seafloor compared to the later casts (Figure 28). This difference in contribution of larger aggregates to total aggregates may have resulted from aggregation of suspended OC26

sediments. A maximum residence time for aggregated suspended sediments in the near bottom suspended layer was calculated to be on the order of 3 days, assuming a suspension height of 100 m and aggregate sinking velocities of 34 m d^{-1}. During this time, bacteria associated with aggregates of suspended sediments may have respired and transformed considerably fractions of sedimentary particulate matter. At the time of sampling, suspended OC26 sediments likely contained oil-carbon and associated substances (e.g. chemical dispersants) from the Deepwater Horizon oil spill in 2010 Thus suspension events of OC26 sediments, like the one observed in the aftermath of Hurricane Isaac, may have periodically transported sediment oil into the overlying water where it could enter microbial food webs.

Conclusions

Hypotheses

Results. The hypothesis that marine snow particles at OC26 would have faster settling velocities than particles at GC600 was not supported; however, the hypothesis that power spectra of particle deposition and current velocities would differ was supported.

APPENDIX A

ILLUSTRATION PERMISSION

Dear Clayton Dike,

Thank you for your request to reproduce IOP Publishing material.

We are happy to grant permission for the use you request on the terms set out below.

Details

Environ. Res. Lett. 7 (2012) 035301 (11pp)

Conditions

Non-exclusive, non-transferrable, revocable, worldwide, permission to use the material in print and electronic form will be granted **subject to the following conditions:**

- Permission will be cancelled without notice if you fail to fulfil any of the conditions of this letter.
- You will make reasonable efforts to contact the author(s) to seek consent for your intended use. Contacting one author acting expressly as authorised agent for their co-authors is acceptable.
- You will reproduce the following prominently alongside the material:
  - the source of the material, including author, article title, title of journal, volume number, issue number (if relevant), page range (or first page if this is the only information available) and date of first publication. This information can be contained in a footnote or reference note; or
  - a link back to the article (via DOI); and
  - if practical and IN ALL CASES for works published under any of the Creative Commons licences the words "© IOP Publishing Ltd. CC BY-NC-SA"
- The material will not, without the express permission of the author(s), be used in any way which, in the opinion of IOP Publishing, could distort or alter the author(s)' original intention(s) and meaning, be prejudicial to the honour or reputation of the author(s) and/or imply endorsement by the author(s) and/or IOP Publishing.
- Payment of £0 is received in full by IOP Publishing prior to use.

If you have any questions, please feel free to contact our Permissions team at permissions@iop.org.

I should be grateful if you would acknowledge receipt of this email.

Kind regards,

Gemma

Please note: We do not usually provide signed permission forms as a separate attachment. Please print this email and provide it to your publisher as proof of permission.

Gemma Alaway
Rights & Permissions Adviser

IOP Publishing
Temple Circus, Temple Way, Bristol
BS1 6HG, UK

Direct line +44 (0)117 930 1146

ioppublishing.org

REFERENCES

25 Years Later: Timeline of Recovery from Exxon Valdez Oil Spill. (2015). *Office of Response and Restoration.* Retrieved from NOAA http://response.restoration.noaa.gov/oil-and-chemical-spills/significant-incidents/exxon-valdez-oil-spill/timeline-ecological-recovery-infographic.html

Acker, J. G., & Leptoukh, G. (2007). Online analysis enhances use of NASA earth science data. *Eos, Transactions American Geophysical Union, 88(2)*, 14-17.

Armstrong, R. H., & Wilson, M. F. (2013). *Natural Connections IN ALASKa.* Nature Alaska Images.

Arnosti, C., Ziervogel, K., Yang, T., & Teske, A. (2014). Oil-derived marine aggregates-hot spots of polysaccharide degradation by specialized bacterial communities. *Deep Sea Research Part II: Topical Studies in Oceanography*.

Berg, R. (2013). *Tropical Cyclone Report Hurricane Isaac (AL092012) 21 August - 1 September 2012.* National Hurricane Center. Retrieved December 29, 2014

Borenstein, S. (2011). BP spill damage runs deep. *Daily Herald (Arlington Heights, IL).* Retrieved from

Crowsey, R. C. (2013). Persistence of Gulf of Mexico Surface Oil from the 2010 Deepwater Horizon Spill. *Southeastern Geographer*, *53*(4), 359-361.

Cruz, V. J. (2014). Assemblage Comparisons of Living Benthic Foraminifera at Bathyal Sites Oiled and Un-oiled by the Deepwater Horizon Blowout in the Northeastern Gulf of Mexico (Masters thesis).

Deep Sea Ecosystem May Take Decades to Recover from Deepwater Horizon Spill. (2013). *U.S. Fed News Service, Including U.S. State News.* Retrieved from Highbeam RESEARCH

http://www.highbeam.com/doc/1P3-3080827091.html

Demes, K., Chang, S., Quayle, M.,Withers, D., Raymond, J., & Stevens, D. Economic and Biophysical Impacts of Oil Tanker Spills Relevant to Vancouver, Canada A Literature Review.

Diercks, A. R., Asper, V. L., Woolsey, M., Jarnagin, R., Dike, C., D'Emidio, M., . . . Conti, A. (2013). Site reconnaissance surveys for oil spill research using deep-sea AUVs. In *Proceedings Oceans Conference* 2013.

Dong, C., Bai, X., Sheng, H., Jiao, L., Zhou, H., & Shao, Z. (2014). Distribution of PAHs and the PAH-degrading bacteria in the deep-sea sediments of the high-latitude Arctic Ocean. *Biogeosciences Discussions*, *11*(9), 13985-14021.

Elliot, D., & Peñaloza, M. (2014, March). Exxon Valdez Oil Spill Brings 'Bad Juju' And Pain 25 Years Later. *NPR.* Retrieved from http://www.npr.org/2014/03/26/294709397/exxon-valdez-oil-spill-brings-bad-juju-and-pain-25-years-later

Exxon Valdez oil spill. (2013). *Water Pollution.* Retrieved from The Encyclopedia OF EARTH http://www.eoearth.org/view/article/152720

Falkovich, G. (2011). *Fluid Mechanics: A Short Course for Physicists.* New York, NY: Cambridge University Press.

Fisher, C. R., Hsing, P.-Y., Kaiser, C. L., Yoerger, D. R., Roberts, H. H., Shedd, W. W., . . . Brooks, J. M. (2014). Footprint of Deepwater Horizon blowout impact to deep-water coral communities. *Proceedings of the National Academy of Sciences of the United States of America*, *111*(32), 11744-11749.

Gardner, W. D., & Walsh, I. D. (1990). Distribution of macroaggregates and fine-grained particles across a continental margin and their potential role in fluxes. *Deep-Sea Research Part A. Oceanographic Research Papers*, *37*(3), 401-411.

Gardner, W. D., Richardson, M. J., Hinga, K. R., & Biscaye, P. E. (1983). Resuspension measured with sediment traps in a high-energy environment. *Earth and Planetary Science Letters*, *66*, 262-278.

Gardner, W. D., Southard, J. B., & Hollister, C. D. (1985). Sedimentation, resuspension and chemistry of particles in the northwest Atlantic. *Marine Geology*, *65*(3), 199-242.

Gulf Oil Spill. (n.d.). *Ocean Portal Find Your Blue.* Retrieved from the Smithsonian National Museum of Natural History http://ocean.si.edu/gulf-oil-spill

Hastings, D. W., Schwing, P. T., Brooks, G. R., Larson, R. A., Morford, J. L., Roeder, T., . . . Hollander, D. J. (2014). Changes in sediment redox conditions following the BP DWH blowout event. *Deep-Sea Research II: Topical Studies in Oceanography*

Hu, L., Yvon-Lewis, S. A., Kessler, J. D., & MacDonald, I. R. (2012). Methane fluxes to the atmosphere from deepwater hydrocarbon seeps in the northern Gulf of Mexico. *Journal of Geophysical Research: Oceans (1978-2012), 117*(C1).

Jouandet, M. -P., Jackson, G. A., Carlotti, F., Picheral, M., Stemmann, L., & Blain, S. (2014). Rapid formation of large aggregates during the spring bloom of Kerguelen Island: observations and model comparisons. *Biogeosciences*, *11*(16), 4393-4406.

Joye, S. B., Teske, A. P., & Kostka, J. E. (2014). Microbial dynamics following the Macondo oil well blowout across the Gulf of Mexico environments. *BioScience, 64*(9), 766-777.

Laine, E. P., Gardner, W. D., Richardson, M. J., & Kominz, M. (1994). Abyssal currents and advection of resuspended sediment along the northeastern Bermuda Rise. *Marine geology*, 119(1), 159-171.

Martinec, C. C., Miller, J. M., Barron, N. K., Tao, R., Yu, K., Stewart, P. M., . . . Landers, S. C. (2014). Sediment chemisty and meiofauna from the northern Gulf of Mexico continental shelf. *International Journal of Oceanography, 2014*.

Mayor, D. J., Sanders, R., Giering, S. L., & Anderson, T. R. (2014). Microbial gardening in the ocean's twilight zone: Detritivorous metazoans benefit from fragmenting, rather than ingesting, sinking detritus. *BioEssays*, *36*(12), 1132-1137.

Oil Remains: The Persistence, Toxicity, and Impact of *Exxon* Valdez Oil. (2014). *Status of Restoration*. Retrieved from Exxon Valdez Oil Spill Trust Council: http://www.evostc.state.ak.us/index.cfm?FA=status.lingering

Passow, U., Ziervogel, K., Asper, V., & Diercks, A. (2012, July 12). Marine snow formation in the aftermath of the Deepwater Horizon oil spill in the Gulf of Mexico. *Environmental Research Letters, 7*(3), 035301

Pemberton, M. (2010, January 18). Oil from Exxon spill still trapped along miles of gravel beaches. *The Charleston Gazette*.

Ploug, H., Terbruggen, A., Kaufmann, A., Wolf-Gladrow, D., & Passow, U. (2010). A novel method to measure particle sinking velocity in vitro, and its comparison to three other in vitro methods. *Limnology and Oceanography: Methods, 8*(8), 386-393.

Ramseur, J. L. (2010, December). Deepwater Horizon Oil Spill: The Fate of the Oil. Washington D.C.: Congressional Research Service, Library of Congress.

Sedimentation and Resuspension Dynamics (n.d.). *The Research*. Retrieved from Ecosytem Impacts of Oil & Gas Inputs to the Gulf http://ecogig.org/research-0#Sedimentation

Shigenaka, G. 2014. Twenty-Five Years After the Exxon Valdez Oil Spill: NOAA's Scientific Support, Monitoring, and Research. Seattle: NOAA Office of Response and Restoration. 78 pp.

Soto, L., Vázquez-botello, A., Licea-durán, S., Lizarraga, M., & Yáñez-arancibia, A. (2014). The environmental legacy of the Ixtoc-I oil spill in Campeche Sound, southwestern Gulf of Mexico. *Frontiers in Marine Scence.*, *1*, 57.

Study: Seafood Safe After Deepwater Horizon. (2012). *NOAA Fisheries*. Retrieved from NOAA: http://www.nmfs.noaa.gov/stories/2012/02/dwhpaper.html

Tansel, B. (2014). Propagation of impacts after oil spills at sea: Categorization and quantification of local vs regional and immediate vs delayed. *International Journal of Disaster Risk Reduction, 7,* 1-8.

Thick Oil Layer Found on Gulf of Mexico Sea Floor. (2010). *U.S./World*. Retrieved from TRIBLIVE http://www.triblive.com/x/pittsburghtrib/news/s_699366.html#axzz3Xgn3LF7H

White, H. K., Lyons, S. L., Harrison, S. J., Findley, D. M., Liu, Y., & Kujawinski, E. B. (2014). Long-Term Persistence of Dispersants following the Deepwater Horizon Oil Spill. *Environmental Science & Technology Letters*, *1*(7), 295-299.